AFRL-RH-WP-TR-2018-0001

MECHANISTIC INTERPRETATION OF HYPOBARIA AND HYPEROXIA USING METABOLOMICS AND PROTEOMICS

Deirdre A. Mahle
Michael C. Moulton
Nadja Grobe
Song Pak
Anthony M. Lowman
Bioeffects Division
Molecular Bioeffects Branch

Molly E. Chapleau
Matthew W. Grogg
Sarah T. Law
Meghan K. Makley
Latha Narayanan
Andrea Hoffman
Henry M. Jackson Foundation for the Advancement of Military Medicine
Molecular Bioeffects Branch
Wright-Patterson AFB OH

Nicholas V. Reo
Angela M. Campo
Wright State University
Department of Biochemistry and Molecular Biology
Dayton OH

October 2017

Interim Report for March 2015 to October 2017

STINFO COPY

Air Force Research Laboratory
711th Human Performance Wing
Airman Systems Directorate
Bioeffects Division
Molecular Bioeffects Branch
Wright-Patterson AFB OH 45433-5707

NOTICE AND SIGNATURE PAGE

Using Government drawings, specifications, or other data included in this document for any purpose other than Government procurement does not in any way obligate the U.S. Government. The fact that the Government formulated or supplied the drawings, specifications, or other data does not license the holder or any other person or corporation; or convey any rights or permission to manufacture, use, or sell any patented invention that may relate to them.

This report was cleared for public release by the 88th ABW Public Affairs Office and is available to the general public, including foreign nationals. Copies may be obtained from the Defense Technical Information Center (DTIC) (http://www.dtic.mil).

MECHANISTIC INTERPRETATION OF HYPOBARIA AND HYPEROXIA USING METABOLOMICS AND PROTEOMICS

(AFRL-RH-WP-TR-2018-0001) has been reviewed and is approved for publication in accordance with assigned distribution statement.

MATTIE.DAVID.R.1230101880 Digitally signed by MATTIE.DAVID.R.1230101880 Date: 2018.01.11 12:24:39 -05'00'

DAVID R. MATTIE
Work Unit Manager
Molecular Bioeffects Branch

MILLER.STEPHANIE.A.1230536283 Digitally signed by MILLER.STEPHANIE.A.1230536283 Date: 2018.02.11 11:59:36 -06'00'

STEPHANIE A. MILLER, DR-IV, DAF
Chief, Bioeffects Division
Airman Systems Directorate
711th Human Performance Wing
Air Force Research Laboratory

This report is published in the interest of scientific and technical information exchange, and its publication does not constitute the Government's approval or disapproval of its ideas or findings.

REPORT DOCUMENTATION PAGE

Form Approved
OMB No. 0704-0188

1. REPORT DATE *(DD-MM-YYYY)*	2. REPORT TYPE	3. DATES COVERED *(From - To)*
31-10-2017	Interim	3/2015 – 10/2017

4. TITLE AND SUBTITLE
Mechanistic Interpretation of Hypobaria and Hyperoxia using Metabolomics and Proteomics

5a. CONTRACT NUMBER
FA8650-15-2-6608

5b. GRANT NUMBER
NA

5c. PROGRAM ELEMENT NUMBER
62202F

6. AUTHOR(S)
Mahle, Deirdre A.*; Moulton, Michael C.*; Grobe, Nadja*; Pak, Song*; Lowman, Anthony M.*; Chapleau, Molly E.[1]; Grogg, Matthew W.[1]; Law, Sarah T.[1]; Makley, Meghan K.[1]; Narayanan, Latha[1]; Hoffmann, Andrea[1]; Reo, Nicholas V.[2]; Campo, Angela M.[2]

5d. PROJECT NUMBER
7757

5e. TASK NUMBER
H0

5f. WORK UNIT NUMBER
7757HD05/H0D1

7. PERFORMING ORGANIZATION NAME(S) AND ADDRESS(ES)
[1]HJF, 2624 Q St, Bldg 851, WPAFB OH 45433-7955
[2]Wright State University, NEC Building 111, 3640 Colonel Glenn Hwy, Dayton OH 45435-0001

8. PERFORMING ORGANIZATION REPORT NUMBER

9. SPONSORING/MONITORING AGENCY NAME(S) AND ADDRESS(ES)
Air Force Materiel Command*
Air Force Research Laboratory
711th Human Performance Wing
Airman Systems Directorate
Bioeffects Division
Molecular Bioeffects Branch
Wright-Patterson AFB OH 45433-5707

10. SPONSOR/MONITOR'S ACRONYM(S)
711 HPW/RHDJ

11. SPONSORING/MONITORING AGENCY REPORT NUMBER
AFRL-RH-WP-TR-2018-0001

12. DISTRIBUTION AVAILABILITY STATEMENT
Distribution A: Approved for public release; distribution unlimited. (MSC/PA-2018-0002; 88ABW-2018-0018, 11 Jan2018)

13. SUPPLEMENTARY NOTES

14. ABSTRACT
The U-2 is an ultra-high reconnaissance airplane that flies as high as 70,000 ft above sea level. Both U-2 pilots and altitude chamber technicians show increased incidence of brain leukoraiosis or white matter hyperintensities (WMH) in T2 weighted magnetic resonance imaging (MRI). The incidence of WMH has been correlated to decreased cognitive function. Pilots of U-2 aircraft fly in cabins pressurized to approximately 30,000 feet and breathe 100 percent oxygen prior to and during flight. It has been hypothesized that exposure to extreme hypobaria, excess oxygen, or a combination of both, irrespective of decompression sickness, is the primary causative factor for these WMH. A rat model was used to examine the cellular and molecular changes caused by extreme hypobaric pressures found at altitude (30,000 feet, 100 percent oxygen) as compared to ambient pressures with 100 percent oxygen (hyperoxic) and ambient pressure with 21 percent oxygen (normoxic). Proteomic techniques identified major up and down-regulated proteins in selected brain regions that were then correlated to biological pathways and cellular functions to highlight key regions of disrupted or modified pathways or cellular functions that have been affected. Nuclear magnetic resonance (NMR)-based metabolomics was used to determine the perturbation in brain lipid profile, which would provide key events associated with white matter changes and effects. ^{1}H (proton)-NMR was used to determine changes in small molecule metabolites to augment the proteomic data, providing more of a systems biology overview. This pilot study offers preliminary evidence of the cellular and molecular changes that occur with hypobaric and hyperoxic exposure.

15. SUBJECT TERMS
U-2, altitude, hypobaria, hyperoxia, white matter hyperintensity, rat

16. SECURITY CLASSIFICATION OF:			17. LIMITATION OF ABSTRACT	18. NUMBER OF PAGES	19a. NAME OF RESPONSIBLE PERSON
U					D. A. Mahle
a. REPORT	b. ABSTRACT	c. THIS PAGE	SAR	40	19b. TELEPONE NUMBER (*Include area code)*
U	U	U			NA

Standard Form 298 (Rev. 8-98)
Prescribed by ANSI-Std Z39-18

THIS PAGE INTENTIONALLY LEFT BLANK.

TABLE OF CONTENTS

LIST OF FIGURES

LIST OF TABLES

THIS PAGE INTENTIONALLY LEFT BLANK.

PREFACE

Funding for this project was provided through the Defense Health Program and the Aerospace Toxicology Program, which is part of the Aerospace Physiology and Toxicology Program in the 711th Human Performance Wing of the Air Force Research Laboratory. This research was conducted under cooperative agreements FA8650-10-2-6062 and FA8650-15-2-6608, both with the Henry M. Jackson Foundation for the Advancement of Military Medicine (HJF). The program manager for the HJF cooperative agreements was David R. Mattie, PhD (711 HPW/RHDJ), who was also the technical manager for this project.

The protocol "Mechanistic Interpretation of Hypobaria and Hyperoxia Using Metabolomics and Proteomics in Sprague Dawley Rats (*Rattus norvegicus*)" was approved by the Wright-Patterson AFB Installation Animal Care and Use Committee (IACUC) as protocol number F-WA-2014-0155. The study was conducted in a facility accredited by the Association for the Assessment and Accreditation of Laboratory Animal Care (AAALAC) International, in accordance with the Guide for the Care and Use of Laboratory Animals (NRC, 2011). The study was performed in compliance with DODI 3216.1.

THIS PAGE INTENTIONALLY LEFT BLANK.

1.0 SUMMARY

The U-2 is an ultra-high reconnaissance aircraft that flies as high as 70,000-feet above sea level. Both U-2 pilots and altitude chamber technicians show increased incidence of brain leukoraiosis or white matter hyperintensities (WMH) in T2 weighted magnetic resonance imaging (MRI) scans, indicative of tissue hypodensities linked to neuronal loss, demyelination and gliotic scarring (McGuire *et al.*, 2012, 2013). The incidence of WMH has been correlated to decreased cognitive function (McGuire *et al.*, 2014). Pilots of U-2 aircraft fly in cabins pressurized to pressure equivalent to approximately 30,000 feet above sea level and breathe 100 percent oxygen prior to and during the flight. It has been hypothesized that exposure to extreme hypobaria, excess oxygen, or a combination of both, irrespective of decompression sickness, is the primary causative factor for these WMH (McGuire *et al.*, 2012, 2013). A mini-pig study was initiated at Lackland AFB with two objectives: 1) Show proof-of-concept that WMH can be induced in a mini-pig model; 2) Gain a better understanding of the pathophysiological changes that are associated with WMH (protocol accession number FWH20130058A). In the Lackland AFB study, mini-pigs were exposed to 100 percent oxygen and hypobaric pressure corresponding to 30,000 feet for several 8 hour periods, similar to the flight profile of a U-2 pilot. Imaging was used to determine if WMH had been induced with pathological analysis follow-up. The research study discussed here aimed to use proteomic and metabolomic techniques in a rat model to examine the early cellular and molecular changes that were caused by similar extreme hypobaric pressures found at altitude (30,000 feet, 100 percent oxygen) as compared to ambient pressures with 100 percent oxygen (hyperoxic) and ambient pressure with 21 percent oxygen (normoxic).

This rodent study was an integrated effort of multiple disciplines to contribute to a mechanistic understanding of the effects of extreme hypobaria and hyperoxia to the pathophysiological studies being conducted in mini-pigs. Proteomic techniques identified major up and down-regulated proteins in brain that were then correlated to known biological pathways and cellular functions to highlight key regions of disrupted or modified pathways or cellular functions that have been affected. Nuclear magnetic resonance (NMR)-based metabolomics was used to determine the perturbation in brain lipid profile, which would provide key events associated with white matter changes and effects. ^{1}H (proton)-NMR was used to determine changes in small molecule metabolites to augment the proteomic data, providing more of a systems biology overview. Because extreme hypobaria and 100 percent oxygen are unique stressors, biochemical assays were used to measure general cellular stress, oxidative stress and inflammation. Specific study goals included:

(a) Set up and execute repeated exposures to ambient, hypobaric pressures (30,000 feet) or hyperoxic conditions using a rodent model.
(b) Complete biochemical assays on brain, heart, lung and blood for lipid peroxidation, stress and inflammation.
(c) Complete proteomic analyses of cortex, hippocampus, cerebellum and brainstem from control and hypobaria/hyperoxia exposed rats.
(d) Characterize the phospholipid and small molecule profiles from extracts of cortex, hippocampus, cerebellum and brainstem from control and hypobaria/hyperoxia exposed rats.
(e) Perform *in silico* pathway analysis to determine changes in cellular/biological functions associated with exposure to extreme hypobaria and hyperoxia.

This pilot study offers preliminary evidence of the cellular and molecular changes that occur with hypobaric and hyperoxic exposure. The data will be used for a power analysis to determine required sample sizes for future studies. The primary limitation of this study was the inability to perform MRI to assess rat brains for a direct correlation to WMH. However, this study fills data gaps involving the mechanistic basis for altered phenotypes in the brain after these extreme exposures, regardless of induction of WMH. Additionally, it has been shown that WMH can be induced with ischemia in the rat brain (Huang *et al.*, 2010). The data has been shared with researchers of the mini-pig study for joint interpretation and determination of necessary follow-on studies. The potential payoff of the knowledge gained from these collective studies is a better approach to defining key pathway(s) activated that could cause WMH for action in mitigating or preventing operational risks and long term adverse health outcomes associated with high altitude flight and operation of altitude chambers.

2.0 INTRODUCTION

The U-2 is an ultra-high reconnaissance airplane that flies as high as 70,000-feet above sea level. Prior to 2012, pilots of U-2 aircraft flew in cabins pressurized to approximately 30,000-feet. Pilots also pre-breathe 100 percent O_2 for 1 hour prior to flight and continue with 100 percent O_2 for the duration of the flight in order to minimize the amount of nitrogen dissolved in the blood and reduce the risk of decompression sickness (DCS). In 2011, increasing tempo of operations saw an increase in neurological DCS (NDCS), prompting medical evaluation of the affected pilots and a follow on study of the U-2 pilot population. The U-2 pilots showed an increased incidence of leukoraiosis or white matter hyperintensities (WMH) in T2 weighted brain magnetic resonance imaging (MRI), indicative of hypodensities linked to neuronal loss, demyelination and gliotic scarring (McGuire *et al.*, 2012, 2013). However, the exact etiology of the lesions is unknown. The incidence of WMH was linked to decreased cognitive function (McGuire *et al.*, 2014). Interestingly, altitude chamber technicians included in this study also had a similar pattern of WMH; these technicians do not experience DCS. It has been hypothesized that exposure to extreme hypobaria, excess oxygen, or a combination of both, irrespective of DCS, is the primary causative factor for these WMH.

A study, headed by Col Paul Sherman, MD and Stephen McGuire, MD of the United States Air Force School of Aerospace Medicine (USAFSAM), was initiated to determine if these same WMH could be formed in a mini-pig model after exposure to hypobaria and hyperoxia. The objectives were two-fold: 1) induce WMH in the mini-pig brain; 2) complete pathohistological examination to determine the nature of the lesions. The mini-pigs were subjected to similar operational conditions as a U-2 pilot – lengthy exposures to hypobaric pressure equivalent to 30,000-feet with 100 percent oxygen, repeated multiple times. The mini-pig study will be reported in a separate publication.

To complement the mini-pig research a preliminary study was designed and completed using a rodent model. Sprague Dawley (SD) rats were exposed to hypobaric conditions equivalent to 30,000-feet with 100 percent O_2 for 4 hr repeated over three consecutive days. A control group was exposed to pressure equivalent to 1000-feet with 21 percent O_2 (normoxic). A third group was added to represent the hyperoxic conditions of 100 percent O_2 at 1000-feet. These research studies used an integrated effort of multiple disciplines to contribute to a mechanistic understanding of the effects of extreme hypobaria and hyperoxia. Proteomic techniques were used to identify major up and down-regulated proteins in brain tissue that can be correlated to biological pathways and cellular functions. Nuclear magnetic resonance (NMR)-based metabolomics analysis was used to determine the perturbation in brain lipid profiles that may be linked to adverse changes in cellular membranes, signaling lipids and myelin-associated lipids. Because extreme hypobaria and 100 percent oxygen are unique stressors, biochemical assays were used to measure general regional brain tissue stress, oxidative stress and inflammation. Corticosterone was measured in serum and in homogenates of each of the four brain regions collected (cortex, cerebellum, hippocampus and brainstem) to characterize generalized stress. Malondialdehyde (MDA) was measured as a marker of non-specific lipid peroxidation, while 8-isoprostane (8-isoP) was measured as a marker of peroxidation of arachidonic acid. Gene expression assays were completed for interferon-gamma (IFN-γ), interleukin-6 (IL-6), tumor

necrosis factor alpha (TNF-α) and nuclear factor kappa B (NFκB) to determine the inflammatory pathways that were activated.

This pilot study offered preliminary evidence of the cellular and molecular changes that occurred with hypobaric and hyperoxic exposure. A limitation with this research was the inability to perform an MRI on the rat brains for a direct correlation to WMH. However, this study aimed to fill data gaps about the early event mechanistic basis for altered phenotypes in the brain after these extreme exposures, regardless of induction of WMH. Understanding the perturbations in biological processes and cellular signaling pathways can help lead to a better understanding of the mechanistic basis for the formation of WMH. This knowledge can be transitioned to improve strategies to mitigate and prevent operational risks and long term adverse health outcomes associated with high altitude flight and operation of altitude chambers.

3.0 METHODS

General methods that pertain to both studies are detailed in Sections 3.1 through 3.5. Specific methods for the acute and two-week studies are found in Sections 3.6 and 3.7, respectively. Method related excerpts from the approved animal use protocol can be found in Appendix A.

3.1 Altitude Chamber Set Up

The altitude system consisted of a custom built 20”x20”x20” stainless steel chamber (Laco Technologies, Salt Lake City UT) with 27 ports and a 1.5” thick acrylic door (Figure 1). The chamber can withstand hypobaric conditions to an equivalent altitude of 50,000 feet. The chamber pressure was monitored from three distributed ports using oxygen cleaned, intrinsically safe, pressure sensors from American Sensors Technology (AST, Mt Olive NJ). A whole body exposure chamber was fitted within the altitude chamber to contain both the rats and the test atmosphere. The test atmosphere was generated using Teledyne mass flow controllers, supplied from compressed gas cylinders, and transported within stainless steel tubing with an inert coating. Immediately upon exiting the whole body chamber, the test atmosphere was mixed with nitrogen such that the vented atmosphere contained no more than 20 percent O_2. The simulated altitude was achieved and maintained by an Edwards 10iC vacuum pump with an inline Aalborg needle valve. Test atmosphere and simulated altitude were controlled via a computer interface with customizable programs created in LabVIEW (Austin TX). For the purposes of this report the term “altitude” refers to the equivalent reduced pressure from sea level pressure.

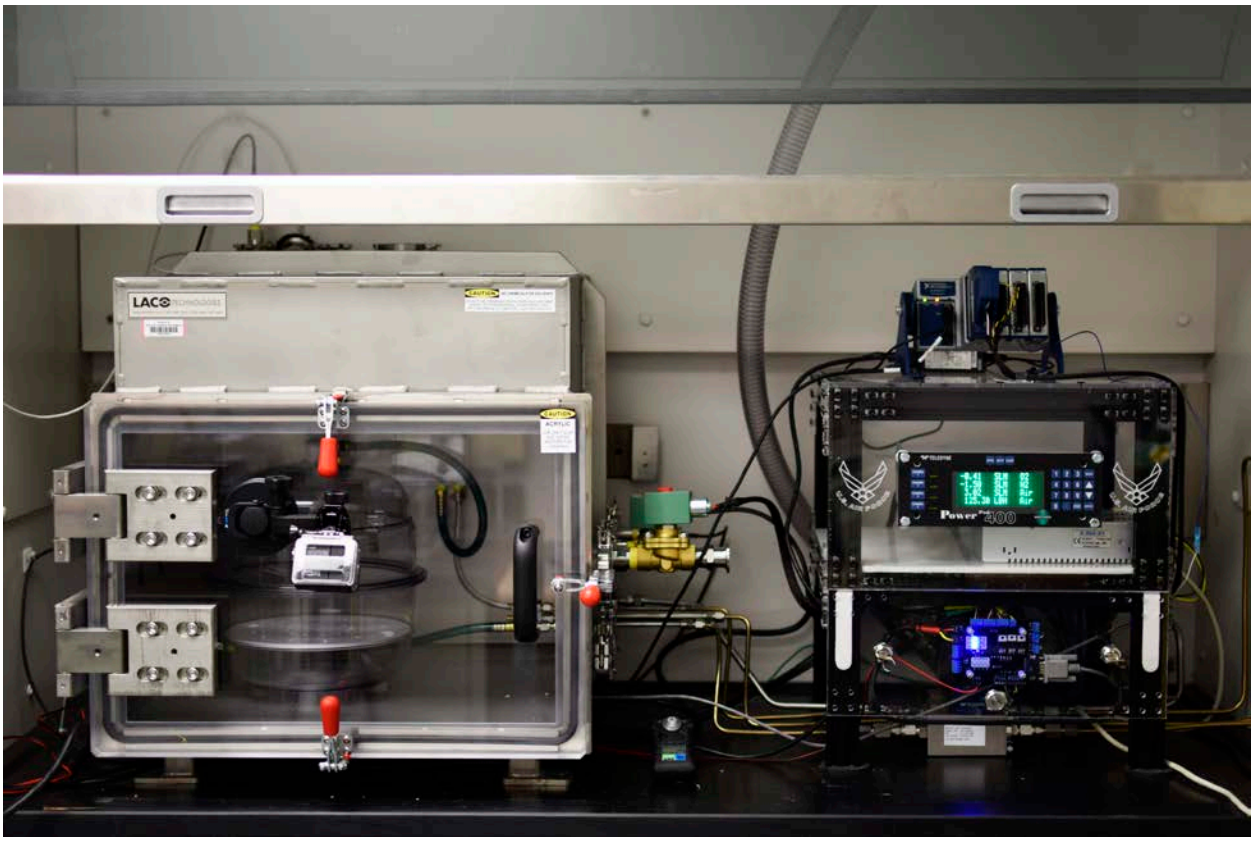

Figure 1. Altitude Chamber System. At left: Stainless steel altitude chamber with interior animal holding chamber. At right: Teledyne mass flow controller with stainless steel tubing transporting gases to altitude chamber.

3.2 Exposure Scenarios

Male Sprague Dawley rats weighing approximately 200 g each were acclimated to the interior holding chamber for 1 hour/day for 3 consecutive days for no fewer than 2 days prior to exposure. The three exposure groups were: 1. Control (CTL) – pressure equivalent to 1000-feet above sea level (14.2 psia) and normal breathing air; 2. Hyperoxia (HYP) – pressure equivalent to 1000-feet above sea level (14.2 psia) and 100 percent O_2; 3. Altitude (ALT) – pressure equivalent to 30,000-feet (4.36 psia) and 100 percent O_2. Two rats were exposed at a time with a total n of 6. Because of the limitations of tissue mass, one of the two rats was used for proteomics and metabolomics and the other rat was used for biochemical assays. For the exposures the two acclimated rats were placed in the interior holding chamber, and the lid was placed and clamped shut. The altitude chamber door was shut and locked. The appropriate program in LabVIEW was initiated for the desired exposure. For altitude exposures, the LabVIEW program was set to increase the altitude 1000-feet/minute. After the 30 minutes ascent, the altitude was maintained at 30,000-feet for 3 hours. After 3 hours the altitude was decreased by 1000-feet/minute. Total exposure time for CTL, HYP and ALT groups was 4 hours. Rats were exposed for three consecutive days. Thirty minutes post exposure on the third day, rats were euthanized via euthanized in accordance with current American Veterinary

Medical Association guidelines (AVMA, 2013). Trunk blood was collected in 15 mL falcon tubes and allowed to clot. Tubes were spun at 2500xg for 10 minutes, and serum was collected. Brains were removed and dissected into cortex, cerebellum, hippocampus and brainstem. Heart and both lungs were also removed. All tissues were flash frozen in liquid nitrogen and stored at -80°C until analysis. All brain regions and tissues were ground under liquid nitrogen in order to provide homogenous sample portions for all assays.

3.3 Mass Spectrometry-Based Proteomics

3.3.1 Sample Preparation. Brain tissue (10 mg) was homogenized in 8 M urea containing 100 mM sodium chloride, 50 mM triethylammonium bicarbonate and 1x Halt protease inhibitor cocktail. The proteins were reduced with 1 mM tris(2-carboxyethyl)phosphine for 30 minutes and alkylated with 15 mM iodoacetamide for 30 minutes in the dark followed by dilution to achieve a 2M urea concentration. Each lysate was quantified using the BCA protein assay kit (Thermo Fisher, Waltham MA) according to the manufacturer instructions. Proteins were digested overnight at 37°C using 3 µg sequencing-grade modified trypsin (Promega, Madison WI). Tryptic digests were evaporated down to a volume of about 150 µl by a vacuum concentrator and acidified to a final concentration of 0.1 percent trifluoroacetic acid. Peptides were desalted using C18 peptide cartridges and evaporated down to a volume of 20 µl by a vacuum concentrator. Samples were neutralized using triethylammonium bicarbonate and samples corresponding to 50 µg protein were labeled using the tandem mass tag (TMT) 10-plex isobaric label reagent set (Thermo Fisher) according to the manufacturer instructions. CTL samples were labeled using 126, 127N, 127C, and 128N tags, whereas for HYP samples 128C, 129N, and 129C tags and for ALT samples 130N, 130C and 131 tags were used. Subsequently, 10 labeled peptide samples were combined, acidified to a final concentration of 0.1 percent formic acid and 100 µg of protein digest was injected into a Waters Spherisorb strong cation exchange (SCX) column (5 µm, 4.6x150 mm). Labeled peptides were eluted with a linear 30-minute gradient of solvent A (25 mM ammonium formate, 15 percent acetonitrile, pH 2.8) to solvent B (525 mM ammonium formate, 15 percent acetonitrile, pH 2.8) at a flow rate of 1 ml/minute. In total, 20 fractions were collected over the entire gradient and each 1.5 ml fraction was evaporated down to a volume of about 200 µl using a vacuum concentrator followed by desalting using C18 peptide cartridges. Desalted peptide fractions were evaporated down to a volume of 20 µl by a vacuum concentrator. Fractions 1-5 and fractions 18-20 were pooled because of a low peptide content. All samples were centrifuged at 14000 rotations per minute (rpm) for 5 minutes and supernatants transferred into high performance liquid chromatography (HPLC) vials for liquid chromatography tandem mass spectrometry (LC-MS/MS) analysis.

3.3.2 Analysis. A total of 14 labeled peptide fractions per brain region were analyzed using a Waters Acquity nanoflow liquid chromatography (LC) system coupled with an LTQ-Orbitrap Velos mass spectrometer (Thermo Fisher). After loading 2 µl of labeled peptide mixture onto a Symmetry C18 nanoAcquity trap column (5 µm, 180 µm x 20 mm) at a flow rate of 8 µl/minute in 0.1 percent formic acid and 1 percent acetonitrile, samples were applied onto a BEH C18 nanoAcquity column (1.7 µm, 75 µm x 200 mm) at a flow rate of 250 nl/minute and 37°C. Peptides were eluted with a step-wise gradient of solvent A: 0.1 percent formic acid in water

versus solvent B: 0.1 percent formic acid in acetonitrile starting at 1 percent solvent B for 3 minutes to 5 percent solvent B at 10 minutes then to 25 percent solvent B at 100 minutes, 65 percent solvent B at 140 minutes, 95 percent solvent B at 150 minutes for 5 minutes and 1 percent solvent at 160 minutes for 20 minutes. The eluent was ionized using an uncoated capillary tip in a NewObjective nano spray ESI source operating in positive ion mode. Ionization voltage was 2.6 kV, and the capillary temperature was 200°C. Mass spectra were acquired in data dependent mode, switching automatically between MS and MS/MS acquisition. All full-scan MS spectra in the range from *m/z* 300 to 2000 were acquired at a resolution of 30000 in the FT-MS and the five most intense ions from each scan were selected for MS/MS analysis in the LTQ using collision-induced dissociation (CID) at 35 percent collision energy for structural information and in the Orbitrap using HCD at 40 percent collision energy for quantitation. The MS/MS automatic gain control (AGC) target setting was 10000 and ion injection time was set to 25 milliseconds.

3.3.3 Data Analysis. The processing of the individual raw MS data files was conducted using a rat protein database in MaxQuant 1.5.8.0 with its integrated search engine Andromeda and target decoy database with a false discovery rate cutoff of 1 percent. Protein intensities were calculated using the algorithms developed for labeled-based quantification by Tyanova *et al.* (2016a). Variable modifications for N-terminal and lysine side chain TMT labeling, methionine oxidation and cysteine carbamidomethylation were included in the database search. Protein intensities were calculated as sum of reporter intensities multiplied by injection time for each isobaric labeling channel for all MS/MS spectra matching to the protein group if a minimum of two peptides were identified of which at least one had to be unique. If a peptide was identified as shared between two proteins (razor), it was used for quantification of the protein group with a larger number of associated proteins or, in the case of a tie, to the protein group with higher-scoring peptides in the Andromeda search. Protein fold-changes of individual HYP and ALT protein intensities were calculated by using the average of pooled protein intensities of the CTL samples as the denominator. Proteins were identified as regulated if the corresponding p values were less than 0.05, based on the one-sample Student t-test, and if the absolute log 2 fold-change of ALT or HYP versus CTL was less than 1. The data were further analyzed through functional interaction network software to understand and visualize the protein pathways that were modulated by hypobaria or excess oxygen. Secondary computational analysis was executed using Perseus 1.5.8.5 (Tyanova *et al.*, 2016b) for statistical rendering.

3.4 NMR-Based Metabolomics

3.4.1 Sample Preparation. Each brain region was extracted by a modified version of the dual phase method of Tyagi *et al.* (1996). Briefly, the study tissues prepared as frozen sample powder were quickly transferred individually to a tared 20 mL glass homogenizer tube, and the weight recorded. Ice cold methanol (MeOH) was immediately added to the tube at 0.7 mL/100 mg tissue, and the mixture was homogenized on ice with a chilled Teflon pestle at 20 rpm (in reverse mode). The homogenate was allowed to stand on ice for 15 minutes. Chilled chloroform ($CHCl_3$) at 0.7 mL/100 mg tissue was added, and the mixture was homogenized at 20 rpm. Chilled double

distilled water (ddH_2O) was added at 0.7 mL/100 mg tissue, and the mixture was homogenized at 20 rpm. The mixture was transferred to an ice cold 50 mL glass centrifuge tube and allowed to stand on ice for 15 minutes before centrifuging at 2000 x g for 25 minutes at 4°C. In the meantime, a separatory flask and funnel were placed in a refrigerator at 4°C. A #1 filter paper disc was placed in the funnel and primed with 0.5 mL each of MeOH, $CHCl_3$ and ddH_2O, in that order. The supernatant was transferred to the flask. The homogenizer tube was washed with 0.5 mL each of MeOH, $CHCl_3$ and ddH_2O and the mixture was re-homogenized. The wash was allowed to stand on ice for 5 minutes, then transferred to the same centrifuge tube and centrifuged at 2000 x g for 5 minutes at 4°C. The supernatant was then added to the separatory funnel. This procedure was repeated three more times. After the supernatant was completely filtered, the mixture was allowed to stand at 4°C for 17-24 hours to allow complete separation of the two liquid phases.

Once separation was complete, the separatory flask was moved to room temperature and allowed to sit for 2 hours. The upper aqueous phase was carefully aspirated with a disposable pipet and transferred to a 60 mL lyophilizer flask. The lower organic phase was drained into a pre-weighed 10 mL amber vial. The separatory flask was washed 3 times with 0.5 mL each of ddH_2O, MeOH, and $CHCl_3$, allowing the solution to sit for 45 minutes between each wash for complete phase separation. Aqueous and organic phases were removed each time as before and added to the same vials from the first separation.

Lipid fraction. The amber vial containing the organic extract was placed in a 25°C water bath, and a gentle stream of nitrogen gas was blown over the top of the vial to evaporate the $CHCl_3$. The vial was then sealed with a black Viton septum (Thermo Fisher Scientific) and placed on vacuum overnight and then weighed. The dried lipid sample was reconstituted in 600 µL of 99.8 percent deuterated chloroform ($CDCl_3$). If the lipid weight was greater than 30 mg, then enough $CDCl_3$ was added to yield a lipid concentration of 50 mg/ml. The vial was crimp-sealed and stored at -20°C until analysis.

Aqueous fraction. The lyophilizer flask containing the aqueous extract was placed in a 25°C water bath and a gentle stream of nitrogen gas was blown over the top of the sample to evaporate the MeOH. After most of the MeOH was evaporated the lyophilizer flask was placed in liquid nitrogen to freeze the aqueous extract and then lyophilized to dryness overnight. The dried aqueous sample was reconstituted in 2 mL of ddH_2O, and 5 g/100 mL of Chelex 100 was added to remove divalent ions. The mixture was stirred at 4°C for 1 hour, then transferred to a 15 mL disposable centrifuge tube and centrifuged at 2000 x g for 10 minutes at 4°C to remove the Chelex. The supernatant was transferred to the original vial, with another 5 g/100 mL of fresh Chelex 100. The mixture was stirred again, at 4°C for 1 hour, transferred to the same 15 mL disposable centrifuge tube and centrifuged at 2000 x g for 10 minutes at 4°C. The supernatant was transferred to a pre-weighed 20 mL clear serum vial and covered with filter paper. The lyophilizer flask was rinsed three times with 2 mL of ddH_2O, transferring each washing to the same centrifuge tube. The tube was centrifuged at 2000 x g for 5 minutes at 4°C, transferring the supernatant to the same vial each time. The vial was placed in liquid nitrogen to freeze the aqueous extract and placed on a lyophilizer overnight. Once dry, the aqueous extract was weighed, crimp-sealed and stored at -20°C for subsequent NMR analysis.

Preparation of samples for NMR analyses. The dried aqueous extracts were reconstituted in 750 µL of 1.04 mM 2, 2`, 3, 3`-deuterotrimethylsilylpropionic acid (TSP) solution prepared in 99.99 percent deuterium oxide (D_2O). TSP was added as a chemical shift reference (set at 0.0 ppm) and internal standard for metabolite quantification (^{1}H NMR). For ^{1}H analysis, 650 µL of the reconstituted solution were added to a 5 mm NMR tube. For NMR analysis, lipid extracts were prepared in a three-part solvent system consisting of $CDCl_3$, MeOH and 90 mM aqueous Cs_2(EDTA) (Meneses and Glonck, 1988). The final lipid sample composition was 12:4:1 $CDCl_3$:MeOH:H_2O (by volume). Samples were placed into 5 mm NMR tubes and a ^{13}C NMR spectrum was acquired first, then triphenylphosphate (TPP) was added to the sample (50 µL of 38 mM TPP in $CDCl_3$) and a phosphorous 31 (^{31}P) NMR spectrum was acquired. TPP provided an internal standard for metabolite quantification. The sample volume was calculated by measuring the height of the lower phase, applying the formula for the volume of a cylinder and correcting for the curvature of the tube bottom.

3.4.2 Analysis. All NMR analyses were performed using a Varian INOVA 600 MHz spectrometer (14.1 T). High-resolution ^{1}H and proton-decoupled ^{31}P and ^{13}C NMR spectra of brain region extracts were acquired in field-lock mode using a 5 mm broadband probe operating at 600, 242 and 150 MHz, respectively. The sample temperatures were maintained at 20°C for lipid extracts to optimize spectral resolution (and minimize evaporation) and 25°C for aqueous extracts. Data acquisition parameters for ^{1}H included 8000 Hz spectral bandwidth, 4 seconds acquisition time, 6 seconds interpulse delay and 1.5 hours of signal averaging. C-13 parameters included a 70° pulse, 36 kHz spectral bandwidth and 4 seconds acquisition time, interpulse delay of 4 seconds, using a waltz ^{1}H-decoupling sequence with nuclear Overhauser enhancement (NOE) and approximately 20 hours of signal averaging. ^{31}P lipid data were acquired with ^{1}H decoupling and NOE using a 90° pulse, 7 kHz bandwidth, 1.9 seconds acquisition time, 3.9 seconds interpulse delay and approximately 18 hours of signal averaging.

3.4.3 Data Analysis. Using a Sun Microsystems computer and VNMR v6.1 software, NMR data were processed using exponential multiplication (0.3 Hz line-broadening for ^{1}H and 1 Hz for ^{31}P and ^{13}C spectra), Fourier transformation, manual phasing and baseline correction (5^{th} order polynomial and spline correction). The ^{1}H and ^{13}C NMR spectra were adaptively binned using a dynamic programming technique in MATLAB® (MathWorks, Inc., R2011b, Natick MA) that sets the minimum distance between peaks to 0.002 ppm and the maximum distance between peaks in a bin to 0.04 ppm (Anderson *et al*., 2010). The less complex ^{31}P spectra from lipid extracts were analyzed using a Gaussian-Lorentzian peak-fitting algorithm available in the VNMR software, which directly outputs peak areas that were used for metabolite quantification.

NMR chemical shift assignments for lipid resonances in the ^{13}C spectrum were taken from the literature (Forgacs *et al*., 2012; Halliday *et al*., 1988; Sillerud *et al*., 1986; and others). The $CDCl_3$ signal was set at 77.79 ppm for reference (relative to trimethylsilane at 0.0 ppm) and was used as the internal standard for quantification. ^{1}H NMR spectra of aqueous extracts and ^{13}C NMR spectra of lipid extracts were analyzed using multivariate data analysis tools, including Principal Component Analysis (PCA) and Orthogonal Projections onto Latent Surfaces Discriminant Analysis (OPLS-DA). Phosphorous NMR of lipid extracts were quantified using

peak area after correcting for T_1 saturation and NOE. This correction was accomplished by acquiring a reference spectrum from a representative sample under conditions of full relaxation with no NOE.

As a first approach PCA and OPLS-DA were used to examine whether treatments influenced metabolite profiles of aqueous brain extracts (^{1}H) and lipid extracts (^{13}C). The ^{13}C spectra can be examined in greater detail by measuring relative changes in various lipid metabolites such as cholesterol, triacylglycerol and some classes of fatty acids (FA) such as n3-FA and n6-FA. The C18, C19 and C14 carbons of cholesterol at 12.5, 19.7 and 57.2 ppm, respectively, were averaged for quantification. The signal in the range of 20.9 – 21.03 ppm represented the n2 carbon from all n3-FA, and the signal within the range of 32.03 – 32.29 ppm represented the n3 carbon of the n6-FA. These carbon signals shift slightly within this range because of the differences in carbon chain lengths of these fatty acids. The terminal methyl carbon of fatty acids at 14.8 ppm was used as a measure of the total FA pool. The signal at 27.3 ppm represented the polyunsaturated fatty acids (PUFA), specifically diallylic carbons, C=C-$\underline{C}H_2$- C=C. While this signal was integrated for a relative quantitative value of PUFA, it is important to note that its intensity is dependent upon both concentration and composition, and, therefore, is not an accurate quantitative measure of concentration.

For quantification purposes the ^{1}H, ^{31}P and ^{13}C NMR signal intensities were corrected for T_1 saturation and NOE, when necessary. To correct for T_1 saturation and NOE data were acquired for a representative cortex and brainstem sample under fully relaxed conditions ($5T_1$ with no NOE; interpulse delay of 250 seconds for ^{13}C and 59 seconds for ^{1}H). The ratio of the intensity of each signal selected to the $CDCl_3$ or TSP intensity was calculated for both fully relaxed (R_{FR}) and partially saturated (R_{PS}) spectra. Calculation of the R_{FR}/R_{PS} ratio provided the saturation factor for each signal of interest. For all analyses metabolite concentrations were normalized to tissue weight.

3.5 Assessment of Stress and Inflammation

3.5.1 Corticosterone Radioimmunoassay - Sample Preparation and Analysis. Assays for corticosterone in rat serum, hippocampus, brain stem, cortex, cerebellum, heart and lung tissues were performed using Immuchem Double Antibody Corticosterone ^{125}I radioimmunoassay (RIA) Kit (MP Biomedicals, LLC, Orangeburg NY). Because serum was collected from all rats regardless of endpoint, the n for corticosterone was 12 not 6. Serum samples were prepared according to manufacturer's standard procedure by diluting 200 times with steroid diluent A. Rat tissue samples were diluted either 200 times or less with diluent A in order to obtain more sensitivity for the detection of corticosterone levels in tissue. The diluted samples were vortexed briefly prior to use. Samples and standards were run in duplicate. Assay kits from the same batch number and with the same expiration date were used for all corticosterone measurements.

3.5.2 C-Reactive Protein ELISA - Sample Preparation and Analysis. Sera were thawed and diluted 1:250,000 in PBS in order to achieve C-reactive protein concentrations within the range

of the standard curve. Rat C-reactive protein (CRP) enzyme linked immunosorbent assay (ELISA, R&D Systems, Minneapolis MN) was performed according to manufacturer's protocol, and optical density (OD) at 450 nm was determined on a FlexStation 3 (Molecular Devices, Sunnyvale CA). OD at 540 nm was subtracted from OD at 450 nm to eliminate background irregularities from the plate. Results were calculated according to kit instructions.

3.5.3 Malondialdehyde - Sample Preparation and Analysis. Approximately 10 mg of each tissue homogenate was lysed via sonication for 15-20 seconds on ice in 303 µL of Lysis Solution. Lysates were centrifuged for 10 minutes at 13,000 x g and supernatants collected. A portion of the supernatant was reserved and used for protein determination (Pierce BCA Protein Assay Kit, Rockford IL). MDA-TBA (thiobarbituric acid) adduct was generated as described in the manufacturer's protocol (Lipid Peroxidation MDA Assay Kit, Abcam, Cambridge MA). The MDA assay procedure was performed in a 95°C bead bath for 60 minutes. Tubes were moved to an ice bath for 10 minutes, then centrifuged briefly to remove precipitate. Supernatant was transferred to wells of a black 96-well plate (Corning, Corning NY) and read on a FlexStation 3 (Molecular Devices, Sunnyvale CA) with Ex/Em = 532/553 nm. Final results were calculated according to manufacturer instructions and final concentrations were reported as pmol MDA/µg total protein.

3.5.4 8-Isoprostane- Sample Preparation and Analysis. Tissue homogenates were weighed into 2 mL polypropylene tubes and placed on ice. Based on the amount of tissue available, the preparation protocol for 8-isoprostane measurement in tissues provided by the manufacturer (Detroit R&D, Inc., Detroit MI) was scaled for average weights of 200 mg for heart, lung and cortex, 50-100 mg of brainstem and cerebellum, and 20 mg of hippocampus. Water was added to each tube (800 µL for heart, lung and cortex; 400 µL for brainstem and cerebellum; 120 µL for hippocampus). A small amount of triphenylphosphine (0.03-0.05 mg/mL; Sigma, St. Louis MO) was added to each sample, followed by ethyl acetate (at a 1:1 volume:volume ratio with water). Samples were extracted three times each with ethyl acetate (Sigma, St. Louis, MO), and supernatants were combined and dried down under nitrogen gas. Samples were dissolved in 20 µL of N, N-dimethyl-formamide (Sigma) by vortexing at room temperature. One-hundred microliters of 1X Sample Dilution Buffer was added to each sample, and mixed well. Fifty microliters of each sample plus 50 µL of 1X Sample Dilution Buffer was added to analysis wells, and ELISA assay was performed as described in the manufacturer's protocol. Absorbance of wells was read at 450 nm on a FlexStation 3 (Molecular Devices, Sunnyvale, CA). Results were analyzed according to kit protocol.

3.5.5 Gene Expression- Sample Preparation and Analysis. ***RNA Isolation.*** Ribonucleic acid (RNA) was isolated from frozen tissue using the Qiagen RNeasy Total RNA System (Qiagen Inc., Hilden, Germany) according to the manufacturer's protocol. RNA was resuspended in 30-50 µl of RNase-free water. RNAs were quantified by the nanospectrophotometer, and 260/A280 ratios greater than 2.0 were considered high purity.

Reverse Transcription (RT). RT was performed using High Capacity complementary deoxyribonucleic acid (cDNA) Reverse Transcription kit (Thermo Fisher Scientific) according to the manufacturer's protocol. Reactions were carried out in 20 µL volumes consisting of 2 µl of 10X RT buffer, 0.8 µl of 25x deoxynucleotide triphosphate (dNTP) mix, 2 µl of 10x RT primers, 1 µL RT, and 4.2 µl nuclease-free water. Reactions were incubated in a polymerase chain reaction (PCR) thermocycler at 25° C for 10 minutes, 37° C for 60 minutes two times, and 85° C for 5 minutes and then cooled to 4°C. After RT, samples were diluted by adding 361 µL of RNase-free water (Thermo Fisher Scientific), making the cDNA concentration equal to ~2.5 ng/µl.

Real-Time Quantitative PCR. Reactions were carried out in 20 µL volumes consisting of 1 µl of 20x TaqMan Gene Expression Assay, 10 µl of 2x TaqMan Gene Expression Assay, 4 µl of RNase-free water, and 5 µL total cDNA. The relative abundance of IL-6, IFN-γ, TNF-α and NFκ-B messenger ribonucleic acid (mRNA) was assessed using TaqMan Assays (5' fluorogenic nuclease assay) to perform real-time quantitative PCR.

4.0 RESULTS

4.1 Biochemical Assay Results

A variety of biochemical assays were completed to characterize the levels of general stress, oxidative stress and inflammation caused by exposure to hyperoxia or altitude relative to control. Corticosterone was measured in serum, all brain regions, heart and lung to quantify the level of generalized stress. CRP is a marker of non-specific inflammation and was assayed in serum only. MDA is a product of lipid peroxidation, and 8-isoP is the peroxidation product of arachidonic acid – both are markers of oxidative stress. IL-6, IFN-γ, TNF-α and NFκB were assayed in all brain regions, heart and lung as markers of inflammation.

Serum levels of corticosterone in the ALT group increased significantly from control ($p<0.05$; Figure 2a). However, the level of corticosterone in each of the brain regions, heart or lung did not change from control (Figure 2b). CRP was assayed in serum only. There were no differences in CRP levels for either the HYP or ALT group (data not shown).

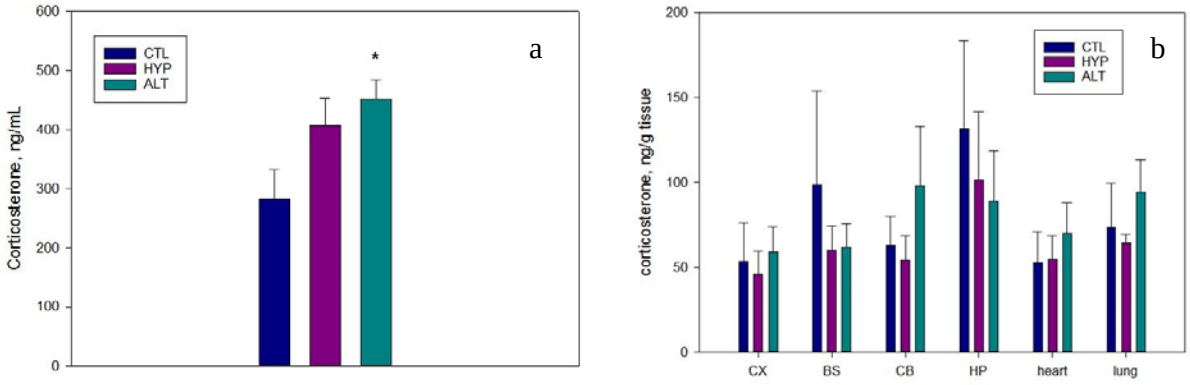

Figure 2. Serum and Tissue Corticosterone Levels. Levels of corticosterone as a marker of generalized stress in hyperoxic (HYP) and hypobaric (ALT) conditions relative to control (CTL); a. serum (normal range for rat: 50-400 ng/mL); b. tissue (CX – cortex; BS – brainstem; CB – cerebellum; HP – hippocampus). Data are mean and standard error of the mean (SEM). Student's t-test (two-tailed) was used to determine significance.

MDA and 8-isoP were assayed in all brain regions, heart and lung. Levels of MDA were no different in either treatment group relative to control (Figure 3) and variability was high. Levels of 8-isoP were significantly lower ($p<0.05$) in heart from the ALT group as compared to CTL (Figure 4). No other tissues showed significance differences in the levels of 8-isoP.

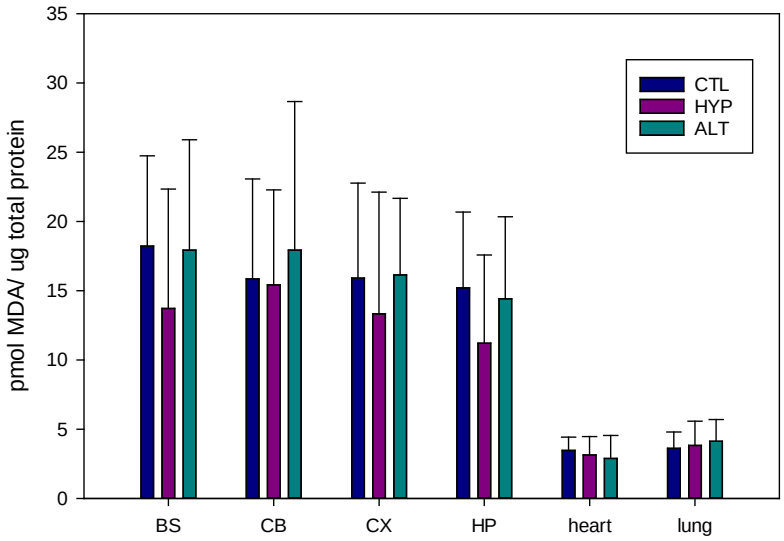

Figure 3. Tissue Levels of Malondialdehyde. Levels of malondialdehyde as a marker of non-specific lipid peroxidation in hyperoxic (HYP) and hypobaric (ALT) conditions relative to control (CTL). CX – cortex; BS – brainstem; CB – cerebellum; HP – hippocampus. Data are mean ± SEM.

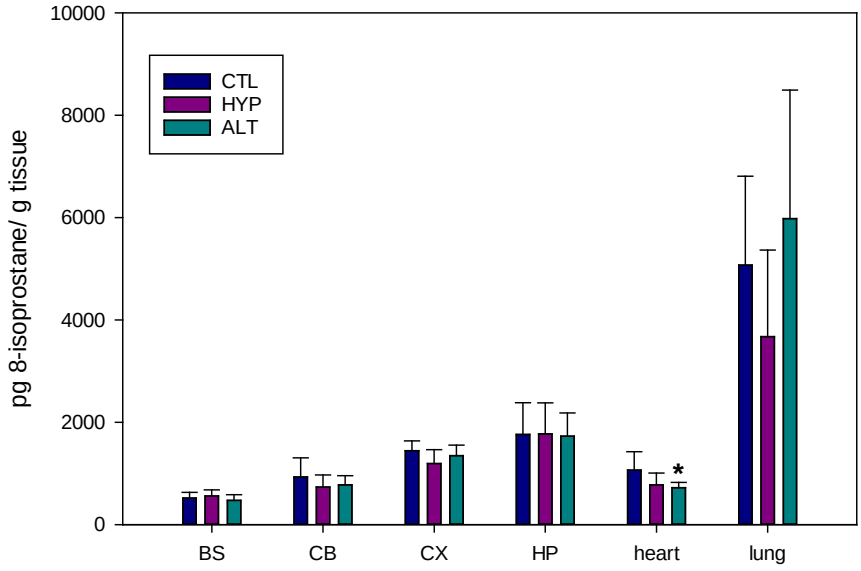

Figure 4. Tissue Levels of 8-Isoprostane. Levels of 8-isoprostane as a marker of arachidonic acid peroxidation in hyperoxic (HYP) and hypobaric (ALT) conditions relative to control (CTL). CX – cortex; BS – brainstem; CB – cerebellum; HP – hippocampus. Data are mean ± standard deviation.

Fold-changes of IL-6, IFN-γ, TNF-α and NFκB relative to control are shown in Figure 5. CTL values were set to 1 and fold-changes were measured relative to CTL. IL-6 (Figure 5a) was decreased in HP and heart for the ALT group while lung levels were increased in that same group. CX and BS showed no difference between treatment groups and control. In the HYP group, BS, heart and lung showed an increase in IFN-γ relative to control (Figure 5b). IFN-γ was also increased nearly two and three-fold in heart and lung, respectively, for the ALT group. Both the HYP and ALT groups had increased levels of TNF-α in HP and lung, but over two-fold-change in the inflammation marker in lung from the ALT group (Figure 5c). NFκB was slightly increased (< two-fold) in BS and HP for the HYP group (Figure 5d). The same marker was also increased in BS from the ALT group.

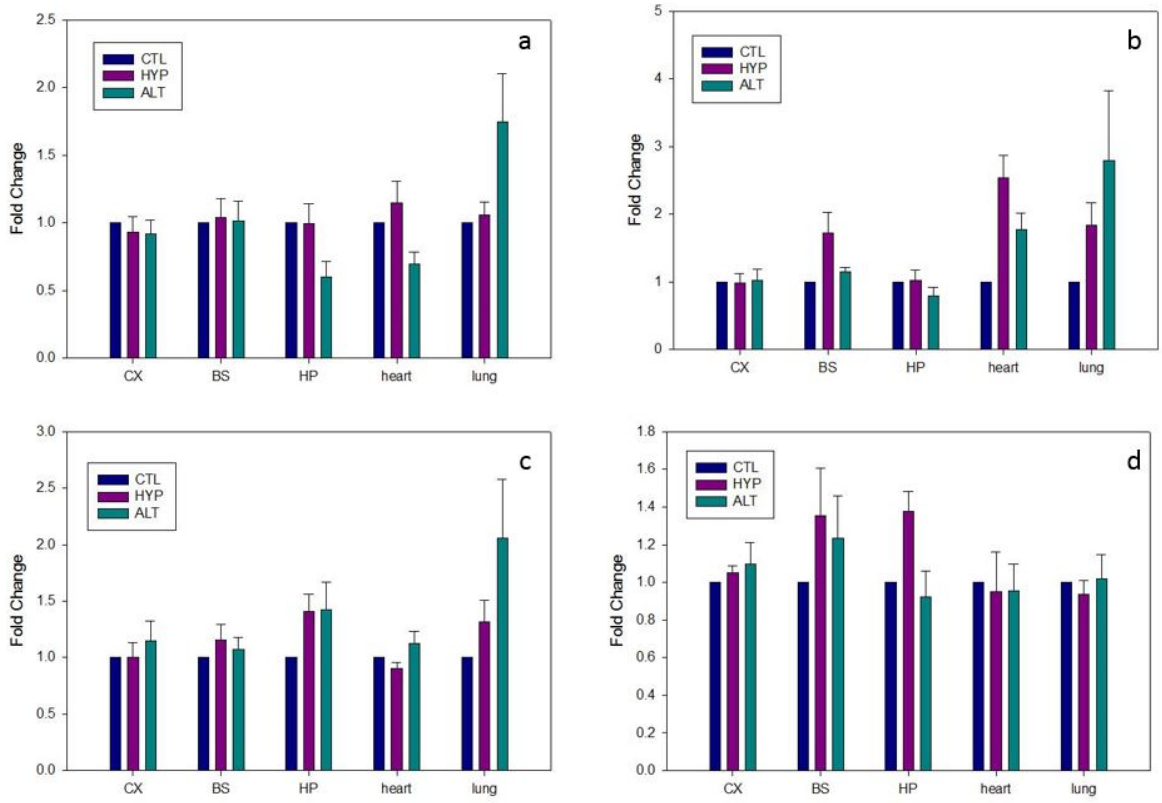

Figure 5. Gene Expression Changes in Markers o Inflammation. Fold-changes in the gene expression of inflammatory markers in hyperoxic (HYP) and hypobaric (ALT) conditions relative to control (CTL); a. IL-6; b. IFN-γ; c. TNF-α; d. NFκB. Data are mean ± SEM. Control values were set to a value of 1. Fold-change was calculated against the controls.

4.2 Proteomic Results

A shotgun proteomics approach, consisting of a TMT labeling strategy and offline fractionation using a strong cation exchange, were applied to quantitatively analyze global protein changes in four brain regions after HYP and ALT exposure. Protein abundances of four biological replicates for the CTL group and three biological replicates per HYP or ALT group were compared each in

two technical replicates using quantitative mass spectrometry. Table 1 summarizes total protein number detected in four brain regions at a false discovery rate of 5 percent ranging from 902 to 1,408 proteins that had quantification values. Results indicate that all brain regions showed similar amounts of identified protein groups as well as a similar number of significantly regulated proteins in the HYP and ALT groups compared with the CTL exposure. Between 0.4-1.7 percent of the total identified proteins were regulated (Table 1).

Hierarchical clustering analysis was performed on all identified proteins. Significant changes in the HYP group were distinct from significant changes in the ALT group for all brain regions and only a small group of regulated proteins showed similar trends (Figure 6). These results suggest that each exposure has a unique protein profile and different modes of action respond to the insult.

Table 1. Summary of Identified and Regulated Proteins in Brain

	Total	**HYP regulated**	**ALT regulated**
HP	902	1	12
BS	942	4	0
CX	1149	8	6
CB	1408	3	21

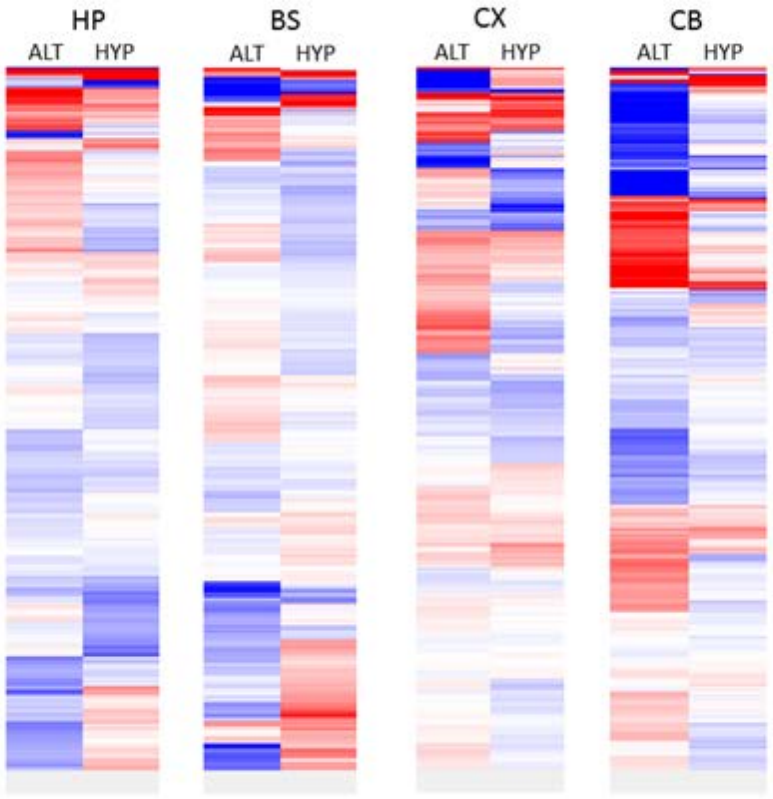

Figure 6. Hierarchical Clustering of Identified Proteins. The heat maps represent log_2 fold-changes of HYP or ALT versus CTL; blue - lower abundance; red - higher abundance. Significantly regulated proteins are represented by bright blue and bright red colors.

Exposure to HYP or ALT resulted in distinct protein profiles for significantly regulated proteins (Figure 7). Numbers of proteins with significantly increased abundance was higher than the number of proteins with decreased abundance in all four regions in both the HYP and ALT groups. The greatest number of significant changes in protein abundance was detected in CB while BS showed the lowest number of significant changes (absolute log_2 fold-change ≥ 0.58, $p \leq 0.05$).

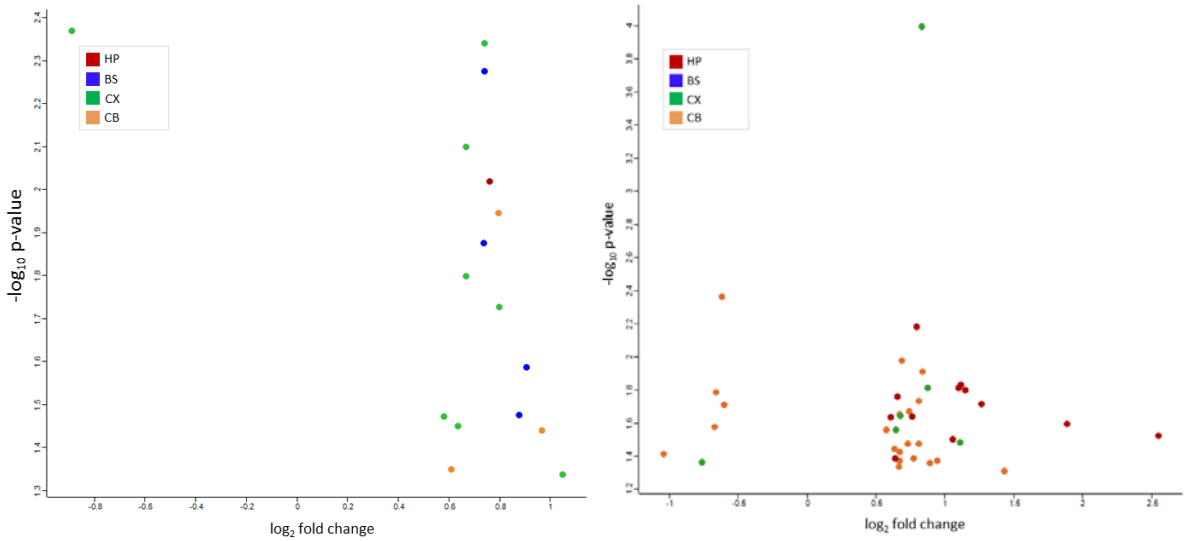

Figure 7. Distinct Protein Profiles in Brain. Protein profiles with altered abundances in HP, BS, CX and CB after HYP and ALT exposure. a. Volcano plot showing significant p values versus normalized protein ratios (absolute $\log_2$ fold-change ≥0.58) in each brain region in the HYP group. b. Volcano plot showing significant p values versus normalized protein ratios (absolute $\log_2$ fold-change ≥0.58) in each brain region in the ALT group.

A list of all significantly regulated proteins per region and exposure is shown in Table 2. There was no overlap between regions. Significantly regulated proteins were unique for HYP and ALT in HP, BS, and CB. However, a similar profile for five significantly regulated proteins, Csde1, Rps21, Rab3gap2, Grm2, and Gpm6a, was identified for HYP and ALT in CX.

Biological processes after HYP and ALT exposure in HP, BS, CX and CB were investigated using the Database for Annotation, Visualization and Integrated Discovery (DAVID, v.6.8; Huang *et al.*, 2009a, b). Gene ontology analysis was performed by combining all significantly regulated proteins for each exposure using the entire genome of R*attus norvegicus*. Gene ontology enrichment revealed proteins in the ALT and HYP groups that were associated with distinct terms (Table 3).

Table 2. Protein Changes in All Four Brain Regions after HYP or ALT Exposure

Protein name	Gene name	Log_2 FC
HP HYP		
Hemoglobin alpha, adult chain 2	Hba-a2	0.75964
HP ALT		
Heat shock 70 kDa protein 1B;Heat shock 70 kDa protein 1A;Heat shock 70 kDa protein 1-like	Hspa1a;Hspa1l	0.60719
Erythrocyte Membrane Protein Band 4.1 Like 2	Epb41l2	0.63891
LETM1 and EF-hand domain-containing protein 1, mitochondrial	Letm1	0.65554
Synaptic vesicle glycoprotein 2B	Sv2b	0.76128
Sodium/calcium exchanger 1	Slc8a1	0.79445
Gephyrin;Molybdopterin adenylyltransferase; Molybdopterin molybdenumtransferase	Gphn	1.05731
Tubulin Alpha Like 3	Tubal3	1.09782
Brain acid soluble protein 1	Basp1	1.11343
Excitatory amino acid transporter 2	Slc1a2	1.14747
Neuronal membrane glycoprotein M6-a	Gpm6a	1.26685
Lymphocyte Antigen 6 Family Member H	Ly6h	1.88709
Myristoylated alanine-rich C-kinase substrate	Marcks	2.54662
BS HYP		
Hemoglobin subunit beta-2	Hbb-b2	0.73697
Protein spinster homolog 1	Spns1	0.73859
Hemoglobin subunit beta-1	Hbb-b1	0.87615
Carbonic anhydrase 1	Ca1	0.90572
CB HYP		
Serine protease inhibitor 2.1;Serine protease inhibitor A3L	Serpina3l	0.60862
Afamin	Afm	0.79563
Fibrinogen gamma chain	Fgg	0.96740
CB ALT		
Acyl-protein thioesterase 1	Lypla1	-1.03881
Neurofilament heavy polypeptide	Nefh	-0.67373
Lanosterol 14-alpha demethylase	Cyp51a1	-0.66032
Myelin-associated glycoprotein	Mag	-0.61993
Myelin proteolipid protein	Plp1	-0.60417
Tumor protein p63-regulated gene 1-like protein	Tprg1l	0.57230
Glycolipid transfer protein	GLTP	0.63204
Alsin	Als2	0.66747
Sodium/potassium-transporting ATPase subunit beta-3	Atp1b3	0.67018
3-hydroxyacyl-CoA dehydrogenase type-2	Hsd17b10	0.67056
Guanine nucleotide-binding protein G(I)/G(S)/G(T) subunit beta-2	Gnb2	0.67240
Filamin-C	Flnc	0.68474
Alpha-enolase	Eno1	0.73153
Proteasome activator complex subunit 1	Psme1	0.73935
D-dopachrome decarboxylase	Ddt	0.77121
Calsyntenin-3	Clstn3	0.80936
Eukaryotic translation initiation factor 3 subunit J	Eif3j	0.81204
Prolyl endopeptidase	Prep	0.83636
Rho GTPase-activating protein 35	Arhgap35	0.89132
Coronin-1B	Coro1b	0.94496
AP-2 complex subunit beta	Ap2b1	1.43301

Table 2. (continued)

CX HYP		
Cold shock domain-containing protein E1	Csde1	-0.88845
Sodium- and chloride-dependent GABA transporter 3	Slc6a11	0.58083
V-type proton ATPase subunit S1	Atp6ap1	0.63550
Metabotropic glutamate receptor 2	Grm2	0.66626
40S ribosomal protein S21	Rps21	0.66859
Rab3 GTPase-activating protein non-catalytic subunit	Rab3gap2	0.74099
Serotransferrin	Tf	0.79690
Neuronal membrane glycoprotein M6-a	Gpm6a	1.04762
CX ALT		
Cold shock domain-containing protein E1	Csde1	-0.76286
40S ribosomal protein S21	Rps21	0.64204
Rab3 GTPase-activating protein non-catalytic subunit	Rab3gap2	0.67629
Metabotropic glutamate receptor 2	Grm2	0.82932
Plasminogen activator inhibitor 1 RNA-binding protein; Plasminogen activator inhibitor 1 RNA-binding protein, N-terminally processed	Serbp1	0.87513
Neuronal membrane glycoprotein M6-a	Gpm6a	1.11181

Note: Shown are protein ID, protein name, gene name and $\log_2$ fold-change (FC) of significantly regulated proteins with absolute $\log_2$ fold-change ≥ 0.58 and $p \leq 0.05$.

4.3 Metabolomic Results

In general, the experimental exposures did not produce consistent results in all animals within a group. It appears that individual animal response was highly variable with some animals responding while others did not. Group effects were not obvious or significant. However, for both the HYP and ALT groups, a subset of animals in each group separated from the remainder of the group, suggesting that these animals were more sensitive to the exposure and had a response.

4.3.1 Brainstem. PCA plots show the separation of individual rats from the ALT group when modeled as ALT versus CTL (Figure 8). All spectra were autoscaled to the CTL spectra for BS to remove any artifacts from the instrumentation. Rats 7 and 19 are shifted far to the right on the first principal component (PC1), while the remaining animals are clustered within a tight scale along PC1 and the second principal component (PC2).

In Figure 9, the spectra are autoscaled to the CTL BS samples and modeled by the HYP and CTL BS spectra. HYP animals 9 and 29 separate along PC1 and PC2 while animal 17 separates along PC2. The PC1 scale is very large, indicating that animals 9 and 29 have very different spectral features in the ^{13}C spectra compared to the CTL BS animals.

Table 3. Enriched Biological Processes after HYP or ALT Exposure using Gene Ontology Analysis through DAVID

Term	Count	%	PValue	Genes	List Total	Pop Hits	Pop Total	Fold Enrichment	Bonferroni	Benjamini	FDR
ALT											
GO:0007416~synapse assembly	3	0.050735667	0.003838148	GPHN, GPM6A, CLSTN3	37	45	17535	31.59459459	0.67466355	0.67466355	4.988864255
GO:0021762~substantia nigra development	3	0.050735667	0.004356313	MAG, PLP1, BASP1	37	48	17535	29.61993243	0.720519332	0.471340689	5.644456537
GO:0043087~regulation of GTPase activity	3	0.050735667	0.007627278	ALS2, RAB3GAP2, ARHGAF	37	64	17535	22.21494932	0.893082982	0.525376819	9.687325916
GO:0061564~axon development	2	0.033823778	0.018330465	PLP1, NEFH	37	9	17535	105.3153153	0.995493166	0.740899718	21.82373195
GO:0042026~protein refolding	2	0.033823778	0.020346903	HSPA1L, HSPA1A	37	10	17535	94.78378378	0.997527615	0.698960675	23.93392997
GO:0048747~muscle fiber development	2	0.033823778	0.03633409	SLC8A1, FLNC	37	18	17535	52.65765766	0.999979745	0.834896557	38.89244726
GO:0006883~cellular sodium ion homeostasis	2	0.033823778	0.040291082	SLC8A1, ATP1B3	37	20	17535	47.39189189	0.999993908	0.820128122	42.14857292
GO:0031668~cellular response to extracellular stimulus	2	0.033823778	0.040291082	SLC1A2, ARHGAP35	37	20	17535	47.39189189	0.999993908	0.820128122	42.14857292
GO:0007268~chemical synaptic transmission	3	0.050735667	0.048480002	AP2B1, GRM2, CLSTN3	37	172	17535	8.266027656	0.999999501	0.836975048	48.38366826
GO:0035249~synaptic transmission, glutamatergic	2	0.033823778	0.05790292	ALS2, CLSTN3	37	29	17535	32.68406337	0.999999973	0.855606379	54.78664214
GO:0021537~telencephalon development	2	0.033823778	0.067551079	SLC8A1, SLC1A2	37	34	17535	27.87758347	0.999999999	0.870266696	60.57495251
GO:0007339~binding of sperm to zona pellucida	2	0.033823778	0.071383385	HSPA1L, HSPA1A	37	36	17535	26.32882883	1	0.859975529	62.67759286
HYP											
GO:0045780~positive regulation of bone resorption	2	0.108873163	0.011858018	TF, ATP6AP1	12	19	17535	153.8157895	0.658223969	0.658223969	12.17037164
GO:0045921~positive regulation of exocytosis	2	0.108873163	0.016812511	FGG, ATP6AP1	12	27	17535	108.2407407	0.78259431	0.53373217	16.8441778

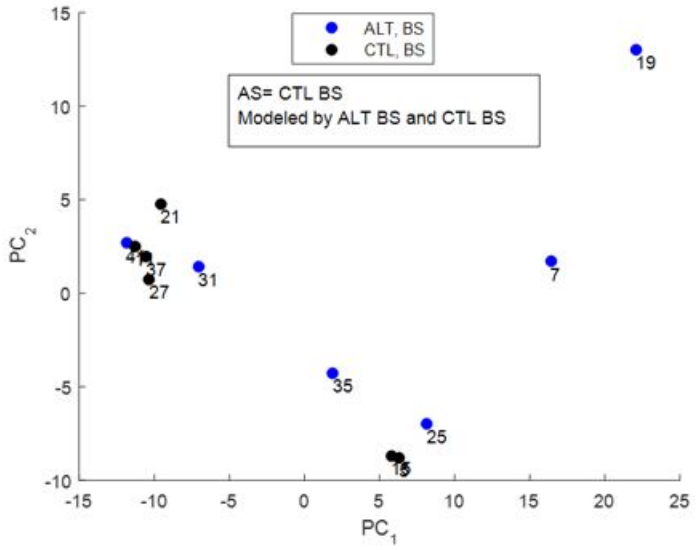

Figure 8. Principal Component Analysis of ALT Brainstem ^{13}C Lipid Spectra. Each numbered symbol represents a ^{13}C lipid spectrum. AS = autoscaling

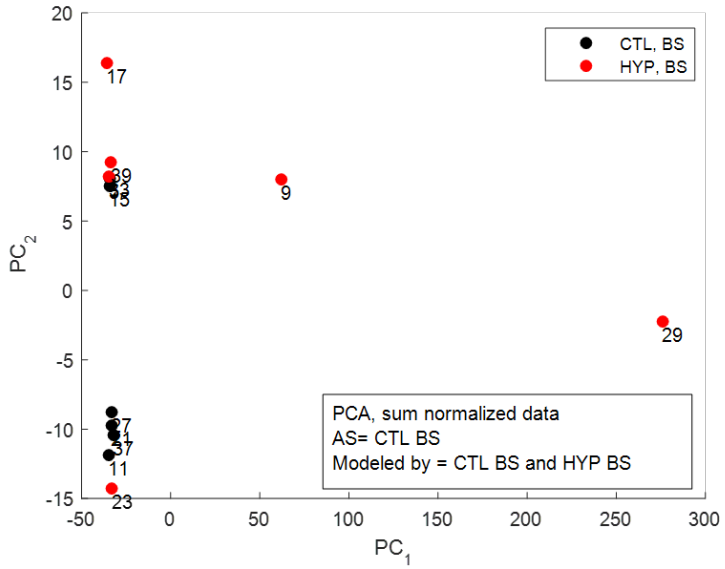

Figure 9. Principal Component Analysis of HYP Brainstem ^{13}C Lipid Spectra. Each numbered symbol represents a ^{13}C lipid spectrum. AS = autoscaling.

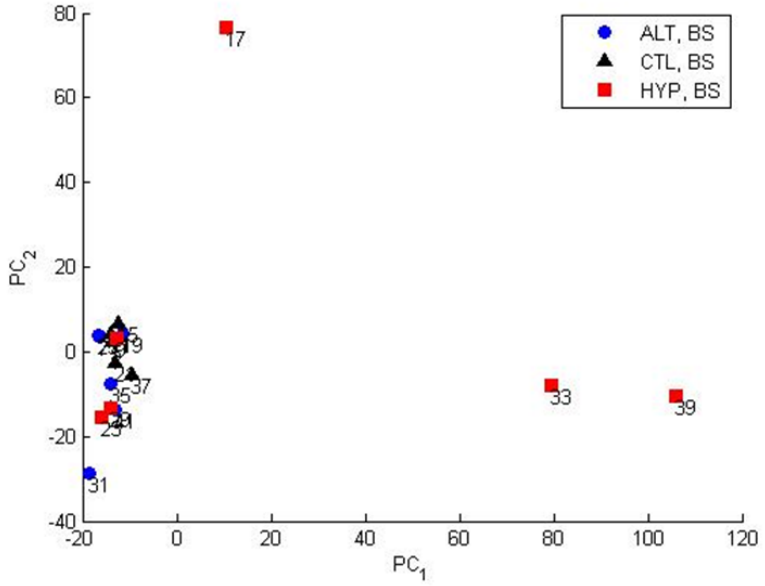

Figure 10. Principal Component Analysis of Brainstem ^{1}H Spectra. Each numbered symbol represents a ^{1}H aqueous spectrum. M = Modeled by; AS = autoscaling.

Figure 10 displays the ^{1}H spectra with rats 17, 33 and 39 from the HYP group separating from the CTL and ALT groups, as well as the remaining HYP group. The CTL, ALT and HYP animals (with the exception of 17, 33 and 39) cluster tightly together along PC1 and PC2.

4.3.2 Cortex. PCA of sum normalized data from CTL and ALT ^{13}C lipid spectra showed clustering of most of the ALT animals with the CTL animals (Figure 11). CTL #37 separates from the cluster along PC2 but not PC1, while ALT #7 separates along PC1 but not PC2. The scale along PC1 is much larger than PC2. Proton spectra of all three groups in a PCA plot shows the majority of the ALT and HYP animals grouping with the CTL (Figure 12); however ALT #41 separates along PC2 and HYP #33 is separated along PC1 which has a relatively large scale.

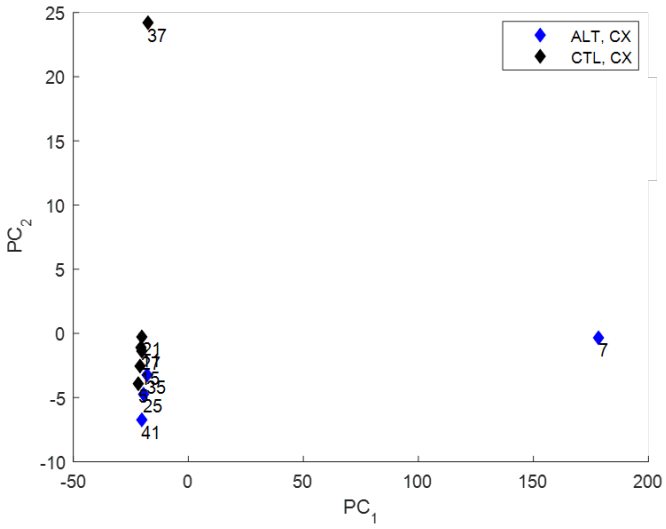

Figure 11. Principal Component Analysis of Cortex ^{31}C Lipid Spectra. Each numbered symbol represents a ^{13}C lipid spectrum. AS = autoscaling.

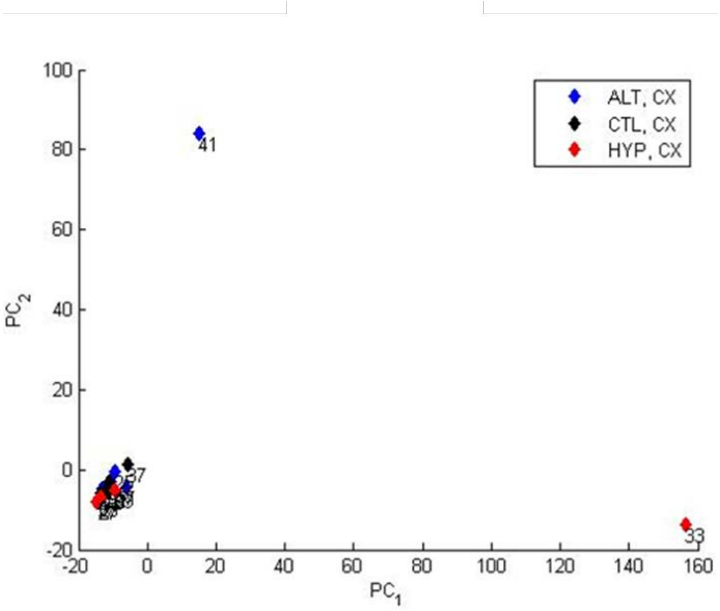

Figure 12. Principal Component Analysis of Cortex ^{1}H Aqueous Spectra. Each numbered symbol represents a ^{1}H aqueous spectrum. M = Modeled by; AS = autoscaling

4.3.3 Cerebellum. PCA plots of the ^{13}C lipid and ^{1}H aqueous data show high variability in the ALT group (Figures 13 - 14). Rats 7, 19 and 35 are displaced from the remainder of the ALT group and from the CTL group along PC1 for the lipid spectra. Rat 19 is also displaced from the rest of the group along PC2. CTL 11 also appears to be different from the other control spectra.

For ^{1}H aqueous data rats 7 and 19 separate from the cluster of ALT and CTL animals along PC1 (both 7 and 19) and PC2 (7).

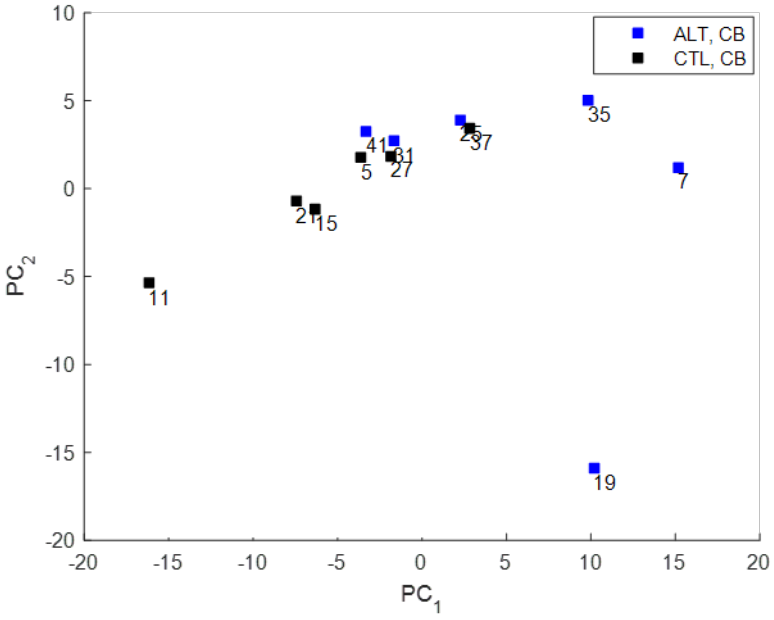

Figure 13. Principal Component Analysis of Cerebellum ^{13}C Lipid Spectra. Each numbered symbol represents a ^{13}C lipid spectrum. AS = autoscaling.

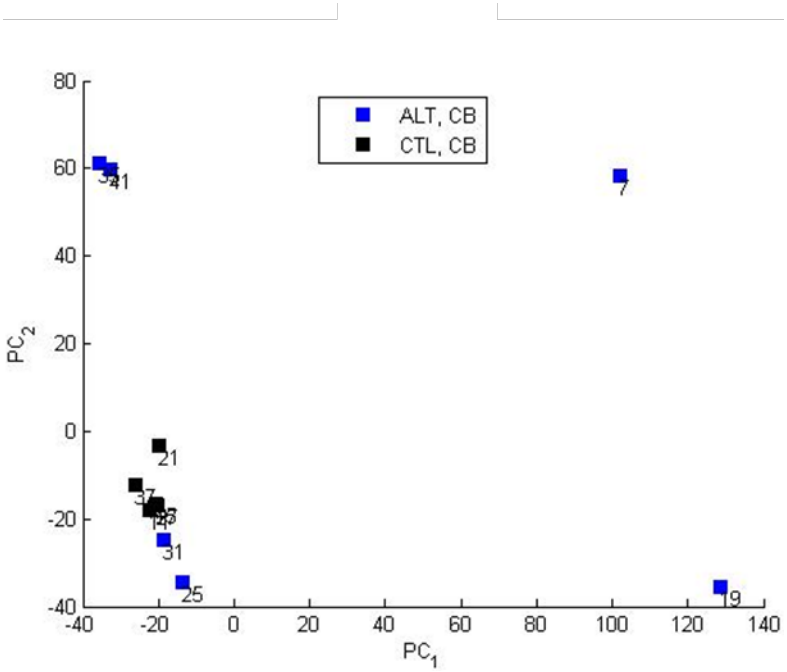

Figure 14. Principal Component Analysis of Cerebellum ^{1}H Aqueous Spectra. Each numbered symbol represents a 1H aqueous spectrum. M = Modeled by; AS = autoscaling.

4.3.4 Lipid Peroxidation. Any animals that were identified as separating from group clusters were examined for lipid breakdown products. Common lipid peroxidation products are usually aldehydes which are alpha to an alkene. All spectra were screened for common peroxidation products. These breakdown products are summarized in Table 4, including the phase in which they are expected to be present. Some compounds may partition into both phases.

Table 5 lists the animals that potentially have lipid breakdown products in the lipid and aqueous phase. HYP BS 29 appears to have HNE in both phases, where other animals only have HNE in one phase.

Table 4. Common Products of Lipid Peroxidation

Compound	Structure	Expected phase
4-Hydroxynonenol (HNE)	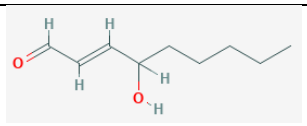	Lipid (~3mg/L water solubility)
MDA	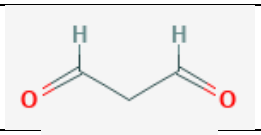	Aqueous
Acrolein	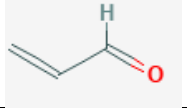	Aqueous Or lipid
9-Oxononanoic acid (9-ONA)	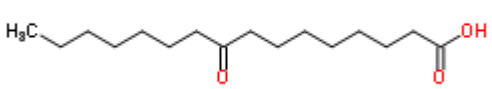	Lipid (~0.005 mg/L water solubility)
4-hydroxyhexanal	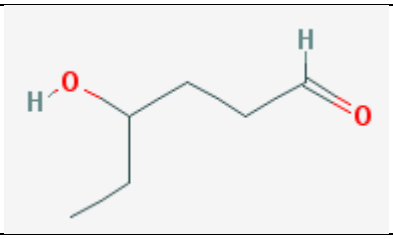	Lipid

Table 5. Animals with Possible Lipid Breakdown Products in ^{13}C and ^{1}H NMR Spectra

Animal	Treatment group/brain region	^{13}C peaks (predicted product)	^{1}H peaks (predicted product) ppm
29	HYP / BS	157.0 ppm (HNE)	9.7 and 6.8 (HNE)
		132.55 ppm (HNE)	9.3 (unknown aldehyde)
		72.6 (HNE)	
		23.45 (HNE)	
	HYP/CX		9.2, 9.1, (unknown aldehydes)
			9.0, 5.7 (MDA)
9	HYP / BS	132.55 ppm (HNE)	
		23.45 (HNE)	
		72.6 (HNE)	
		39.2 ppm (corticosterone)	
	HYP/CX		9.3, 9.2, 9.1 (unknown aldehydes)
33	HYP/CX		9.3, 9.2, 9.1 (unknown aldehydes)
39	HYP/HC		9.3, 9.2, 9.1 (unknown aldehydes)
	HYP/CB		9.3, 9.2 (unknown aldehydes)
17	HYP/CB		9.3 (unknown aldehyde)
	HYP/CX		9.3, 9.2, 9.1 (unknown aldehydes)
			9.0, 5.7 (MDA)
7	ALT / CX	39.19 ppm (corticosterone)	
	ALT/BS	72.6 (HNE)	
		132.55 ppm (HNE)	
19	ALT/BS	72.6 (HNE)	
		132.55 ppm (HNE)	
	ALT/CX		9.3, 9.2, 9.1 (unknown aldehydes)
			9.0, 5.7 (MDA)
25	ALT/BS	72.6 (HNE)	
		132.55 ppm (HNE)	
	ALT/CX		9.3, 9.2, 9.1 (unknown aldehydes)
35	ALT/BS	72.6 (HNE)	
		132.55 ppm (HNE)	
	ALT/CB		9.3, 9.2 (unknown aldehydes)
	ALT/CX		9.3, 9.2, 9.1 (unknown aldehydes)
41	ALT/BS		9.7 (HNE)

			9.3 (unknown aldehyde)
	ALT/CB		9.3, 9.1 (unknown aldehydes)
	ALT/CX		9.3, 9.2, 9.1 (unknown aldehydes)
31	ALT/BS		9.7 (HNE)
	ALT/CX		9.3, 9.2, 9.1 (unknown aldehydes)

Omega-3 and omega-6 FA are prime targets for oxidation because of their carbon-carbon double bonds. The peaks for omega-3, omega-6, chloroform, total fatty acid pool via the terminal methyl peaks, and cholesterol peaks were integrated using the Varian VNMR software. Each peak integral was divided by the chloroform integral, as chloroform acts as an external standard since the concentration is known in each sample. Ratios for omega-3/total FA pool, omega-6/total FA pool and cholesterol/total FA pool were calculated and bivariate analyses were completed (Figure 15). For this analysis, all brain regions were combined to determine the effect based on treatment alone. For example, the ALT plot contains all ALT animal BS, CB, and CX samples. ALT and CTL show clear positive correlation while HYP does not.

The relationship between 4-HNE and omega-3 or omega-6 FA was investigated. For these analyses, the 4-HNE peak in the ^{1}H spectra was integrated and divided by the integral for TSP, an external standard. No overall correlation was detected; however, it appears that there were some samples in each treatment group that have low omega-3 FA when 4-HNE is present (Figure 16).

Figure 17 displays the relationship between omega-6 FA and 4-HNE. These data are very similar to Figure 16 in that omega-6 FA are low when 4-HNE is present but are presenting lower values when 4-HNE is absent. It appears that, in general, omega-6 FA are higher in CTL than ALT.

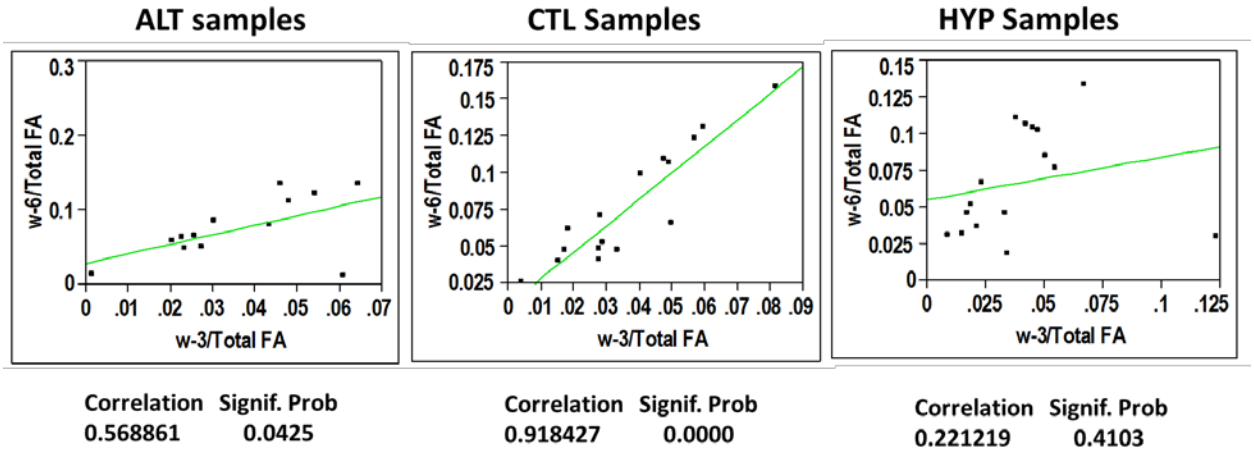

Figure 15. Bivariate Analysis of Omega-3 and Omega-6 Fatty Acids

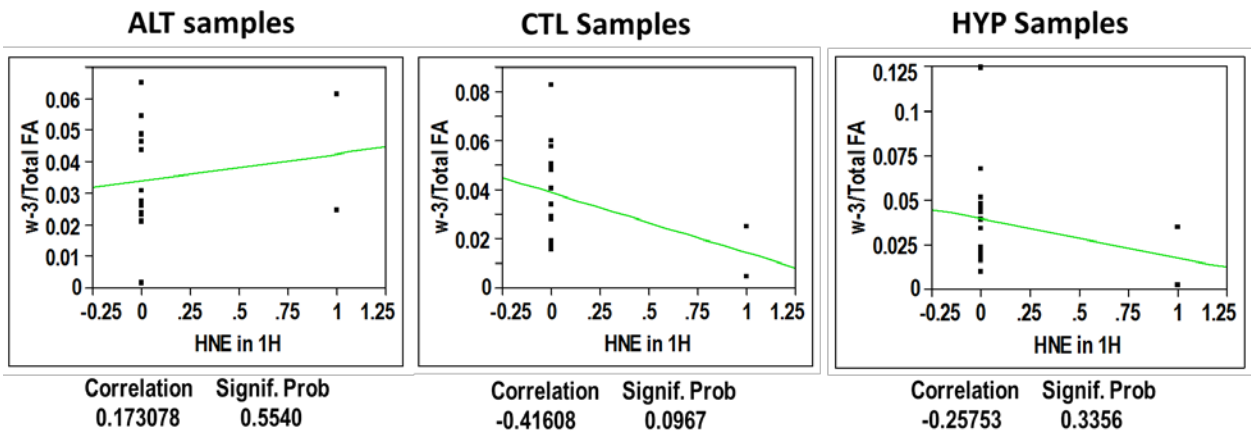

Figure 16. Bivariate Analysis of Omega-3 Fatty Acids and the Presence of 4-HNE

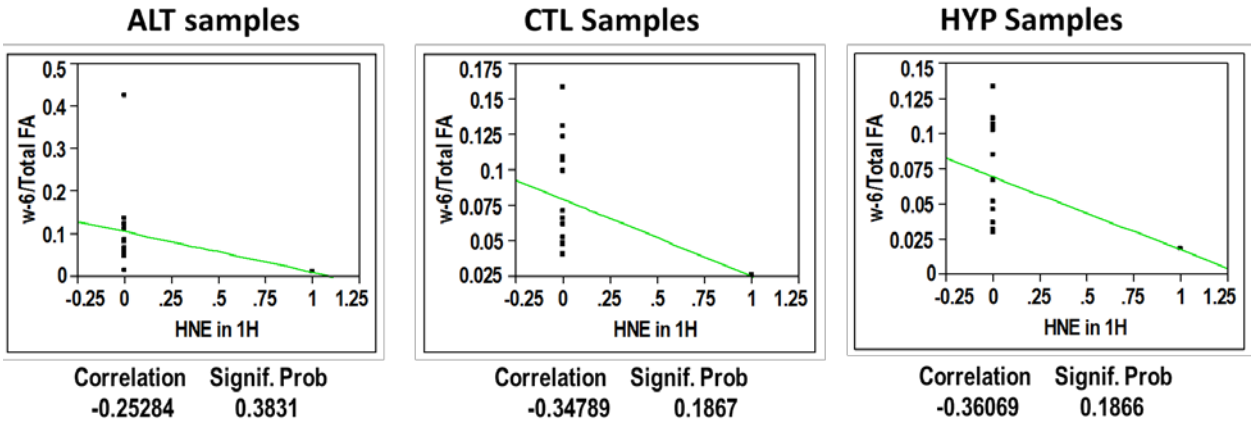

Figure 17. Bivariate Analysis of Omega-6 Fatty Acids and the Presence of 4-HNE

While cholesterol cannot be oxidized to 4-HNE, levels of cholesterol can be affected by changes in the cellular redox balance. Therefore, the relationship between cholesterol and 4-HNE was also determined. Bivariate analysis of cholesterol and 4-HNE produced significant results in all treatment groups (Figure 18). When 4-HNE is present, cholesterol is reduced.

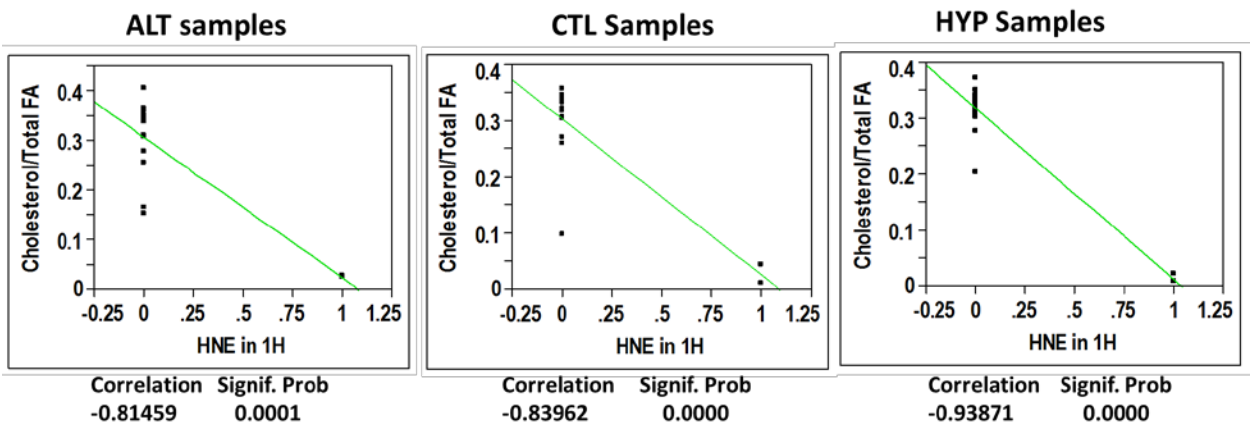

Figure 18. Bivariate Analysis of Cholesterol and the Presence of 4-HNE

5.0 DISCUSSION

This report details the findings of a preliminary study investigating the effects of hypobaria on cellular and molecular functions in brain, using a rat model. A multi-disciplined, systems biology approach was used to elucidate the potential mechanistic basis of adverse effects caused by exposure to extreme stressors experienced by high altitude pilots, namely hypobaria and hyperoxia. The rat model was chosen to complement the research efforts conducted in mini-pigs at USAFSAM. It is recognized that the rat brain is different in size, structure, and vasculature from the human brain and, therefore, not the perfect model for investigating the induction of WMH. While not an exact representative model of the human brain, the individual cellular genetic and protein pathway responses causing an altered phenotype to the stressors of hypobaria and hyperoxia can be comparable between species. Likewise, if there are regional differences in the effects of hypobaria or hyperoxia (hippocampus versus cerebellum), those changes should be quite similar as well. In support of selection and use of the rat model, it is known that WMH can be induced in a rat model after an ischemic event, which in part causes lack of oxygen in the brain (Huang *et al.*, 2010).

Proteomics was selected because it is a powerful tool that can link altered proteins to discrete signaling pathways, cellular functions and regions of the cell. Lipid NMR-based metabolomics offers critical insight into all lipid species. Because the WMH appear to be localized to the peri-axonal regions, lipids are of particular interest as they define cellular structure, protection and signaling. A number of biochemical assays were performed to determine any induction of stress, oxidative stress or inflammation, in order to describe more wholly the nature of the neurocellular insult caused by these whole body exposures.

SD rats appeared to be fairly tolerant of the exposure conditions. All rats maintained typical behavior patterns, including exploring their new environment, grooming and ultimately sleeping. Similar tolerance was seen with the mini-pigs (Sherman, P. Personal communication). As a possible result of this tolerance, the effects seen from this preliminary study were likely lower in overall magnitude. However, corticosterone levels in serum were significantly elevated in the ALT group relative to control. Despite outward appearances, these rats were experiencing stress

as a result of the exposures. The serum levels of corticosterone in the HYP group were elevated from CTL, but not statistically significant.

Exposure to 100 percent oxygen is considered to be potentially toxic. The HYP group was added to attempt to separate the effects of high levels of oxygen from the effects caused by hypobaria. This is, essentially, impossible to do precisely because hypobaric exposure without a corresponding increase in oxygen causes a hypoxic condition. However, by adding a HYP group, it may be possible to identify some effects that are not seen in the ALT group and attribute those to the oxygen toxicity. Indeed, proteomics results indicate that effects seen in the ALT group are different from effects seen in the HYP group except for CX, where similar protein profiles were identified. The lipid-rich environment of the brain makes it a vulnerable target for oxidative stress, manifesting as lipid peroxidation. The adverse effects of lipid peroxidation include a decrease in membrane fluidity with a corresponding increase in membrane leakiness, as well as damage to the many membrane proteins, including receptors, transporters, enzymes and ion channels (Halliwell, 2006). Proteomics results revealed that the abundance of selected membrane proteins were affected by ALT exposure but not HYP exposure. For example Slc8A1, a sodium-calcium exchanger that removes calcium from the cells in exchange for the import of three sodium ions, was upregulated in the ALT group of HP. Interestingly, extracellular calcium was shown to play a major role in mediating white matter damage induced by trauma (Stys *et al.*, 1990). Similarly, the principal transporter for glutamate and aspartate, Slc1a2, was upregulated in the ALT group of HP. A recent study showed a significant increase of this amino acid transporter in deep white matter of chronic human ischemic brain tissue suggesting a possible role in white matter damage (Yatomi *et al.*, 2013). However, levels of MDA and 8-isoP were not significantly elevated in any of the selected brain regions. MDA levels in brain were highly variable, preventing any observation of slight or moderate peroxidation. Heart and lung were considered to be potential target organs for oxygen toxicity, and thus were also assayed for markers of lipid peroxidation. The variability of 8-isoP in the lung was high, and any observation was not statistically significant. Levels of 8-isoP in the heart of rats in the ALT group were significantly lower than CTL, possibly because of the extremely low partial pressure reducing the amount of the oxygen dose. Future studies should include a measure of enzymatic antioxidants (catalase, hydrogen peroxidase and superoxide dismutase) as early indicators of a cellular response to oxygen toxicity and oxidative stress. These indices may be more sensitive markers of oxygen toxicity.

Inflammatory pathways are often triggered as a result of some perturbation or injury. Therefore, it was important to determine if inflammation played a role in hypobaric insult. Gene expression of IL-6, IFN-γ, TNF-α and NFκ-B, known markers of inflammation was measured and reported as a fold-change from control. IL-6 is a pro-inflammatory marker that is capable of stimulating an immune response. Interestingly, it can also inhibit TNF-α. The cytokine IFN-γ activates both innate and adaptive immune responses. TNF-α is a pro-inflammatory cytokine which is released primarily in response to severe brain injury such as ischemia, trauma, and excitotoxicity (Raivich *et al.*, 1999). Elevated levels of TNF-α are present in spinal cords of rodent models of neurodegenerative disease, suggesting that TNF-α is a driver of neuroinflammation and may play a role in the etiology (Hensley *et al.*, 2003). The protein NFκ-B is ubiquitous in most cells and plays a role in the response to stress (Gilmore, 2006), and is part of an initiating stress pathway to elicit TNF-α production.

As previously stated, all changes were of low magnitude, likely reflective of the moderate exposure conditions. IL-6 showed changes in the ALT groups only (HP, heart and lung) with less than a 2-fold difference from control. However, these data are currently inconclusive. IFN-γ, though, does show a trend toward more substantial increases in fold-change relative to control for BS, heart and lung, particularly for the HYP group. It appears that this cytokine may play a role in the response to both hyperoxia and hypobaria. TNF-α only showed increases in expression in HP and lung for both the HYP and ALT groups. The lung is an obvious direct target of hyperoxia and hypobaria. The increase of TNF-α in this tissue may suggest that a pro-inflammatory response has been initiated. The fold-change for the ALT group is higher than that for the HYP group. It is unclear, though, if the increase in expression of this cytokine is triggered by the high levels of oxygen and then again by the hypobaric conditions, as the level of oxygen at simulated 30,000-feet is not significantly higher than 21 percent. HP was the only brain region to show an increase in TNF-α, although the fold-change was less than two. This finding warrants further investigation with an exposure of increased intensity to determine if there is a corresponding increase. As the center of learning and memory, the HP should be considered to be a sensitive region of the brain. Being responsive to stress, it was anticipated that NFκ-B would be activated in response to both the HYP and ALT exposures, particularly since the corticosterone data indicated that the animals were indeed stressed. However, only BS and HP showed an increase in NFκ-B, and the changes were slight. Overall, the subtle changes in inflammatory markers are suggestive of a mild response to the exposure conditions. Future work should include an exposure scenario that increases the duration and number of repeats in order to augment the response and highlight the true nature of the injury. It is interesting to note that CX showed essentially no changes in any of the markers. Perhaps this is related to the presence of more grey matter than white matter or that CX is more resistant to the exposure conditions.

Overall, the proteomics data revealed mild effects of HYP or ALT exposures with less than 2 percent of the proteins differentially regulated across all four brain regions. In order to determine these minimal changes, a newly optimized proteomics workflow, including pre-fractionation of TMT-labeled samples and a stepwise LC gradient, had to be developed prior to data acquisition. A robust and reliable LC-MS/MS approach is the prerequisite to uncover changes in protein profiles, especially for exposures where only moderate changes are expected, or for proteins with low abundance. A comparison to data obtained without pre-fractionation or with using a linear LC gradient revealed that less than half of the total amount of proteins were identified (data not shown). Using the optimized proteomics strategy, significantly regulated proteins showed a trend towards increased abundance in all brain regions suggesting activation of feedback mechanisms to counterbalance the moderate hypobaric and hyperoxic stimuli. More proteins were changed in the ALT group as compared to the HYP group for all brain regions combined, which indicates that the ALT exposure resulted in more of a phenotypic change than HYP exposure. In addition, significant changes in protein abundance were unique between HYP and ALT suggesting distinct molecular effects resulting from each exposure scenario. CB showed the highest total number of differentially regulated proteins, which could be partially due to a higher total number of identified proteins. Future work using more animal numbers and a longer exposure protocol will aid in identifying the mechanistic basis of the injury and the brain region that is affected most by hypobaria and/or hyperoxia.

The NMR data were similar to the other data sets in that changes were mild and highly variable. However, when analyzed by PCA the spectral data showed very interesting patterns of clustering and separation. The interpretation of these PCA plots was that some animals were responders to hypobaria or hyperoxia while others were not. Table 6 shows the list of animals that may be potential responders to hyperoxia and hypobaria.

Table 6. Animals Identified in PCA Plots as Potential Responders

Treatment and tissue	Potential responders
ALT BS	7, 19 Potentially 41 & 31
HYP BS	29, 9, 17, 23
ALT CB	7, 19, 35
HYP CB	17, 29
ALT CX	7
HYP CX	33, 39, 9
Common across multiple brain regions	ALT 7, 19 HYP 17, 29, 9, 33, 35

Animal 7 from the ALT group was consistently separated from the other animals in that group and from control in CX, BS and CB. ALT 7 also had the highest serum corticosterone levels at 607 ng/mL, providing evidence that this rat had an adverse response to the hypobaric exposure; normal levels for the rat range from 50-400 ng/mL. Several rats with high serum corticosterone levels were also identified as separating from the rest of their treatment group, including ALT 41 (BS) and HYP 9 (BS), 29 (BS, CB), 33 (CX) and 39 (CX). However, ALT 19 and 31 also separated from their respective groups but had a serum corticosterone level within the normal range, further highlighting the inconsistent results involving differential response across individuals. Spectra from several animals listed in Table 6, however, showed the presence of lipid peroxidation products. It appears that there is some correlation between the presence of 4-HNE, a lipid peroxidation product, and omega-3 and omega-6 FA. Their carbon-carbon double bonds make these FA prime targets for oxidation at the α-carbon. 4-HNE can be formed from both omega-3 and omega-6 FA, is a toxic compound and should be at low levels in a healthy cell. 4-HNE is a strong electrophile that can react with the double bonds in deoxyribonucleic acid and proteins. It can also deplete cellular antioxidants, further increasing oxidative stress (Zhi-Hua and Etsuo, 2006). While several samples have low omega-3 FA when 4-HNE is present, the instances where omega-3 FA are low in the absence of 4-HNE indicates that this is likely not the sole mechanism for reduction of omega-3 FA.

Omega-6 FA show similar patterns as the omega-3 FA. Omega-6 FA are reduced in treatment groups but the breakdown products of peroxidation species are not being detected. The animals may clear the toxic products quickly, the breakdown products may be below the limit of detection or the breakdown products may be a different compound not yet identified in the spectra. Future studies should include NMR analysis of known standards of peroxidation products in order to determine potential oxidative species or formation of by-products.

The significant negative correlation of cholesterol and 4-HNE was very interesting, particularly because there is no direct link between these two compounds. Cholesterol cannot be oxidized to produce 4-HNE. However, it appears that cholesterol is sensitive to the altered redox balance in the cell. The loss of cholesterol could indicate that the cell membrane permeability has been compromised or that myelin has been damaged. Cholesterol loss in the brain has been implicated in reduced vesicle recycling by presynaptic neurons, as well as reduced vesicle fusion and release. In postsynaptic neurons cholesterol loss impairs long term potentiation, resulting in memory and learning deficits (Bjorkhem and Meaney, 2004). Unknown peaks in the ^{13}C spectra near cholesterol were noted (Figures 19 a, b). These unknown peaks could represent cholesterol breakdown products. Follow on studies should attempt to verify the nature of these peaks to determine if they are, in fact, breakdown products of oxidized cholesterol.

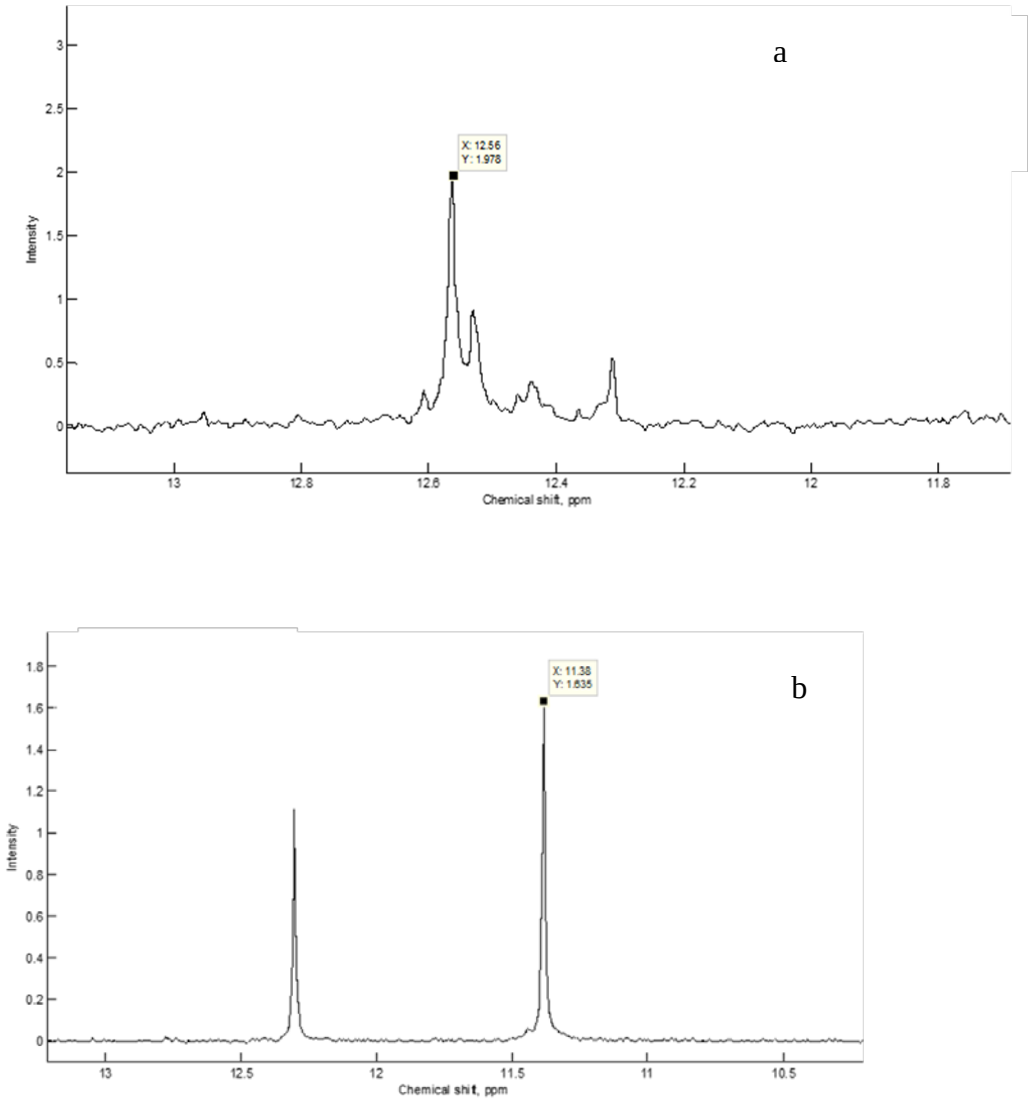

Figure 19. Examples of Unknown Peaks near Cholesterol. a. Unknown peaks near cholesterol (12.31 ppm) in CTL BS 37; b. Unknown peak (11.38 ppm) upfield of cholesterol in HYP BS 9.

Overall, these data suggest that lipids were oxidatively damaged as a result of both the HYP and ALT exposures. Hyperoxic exposure has been shown to result in oxidative damage when used as a treatment for stroke, traumatic brain injury or cardiac arrest (Vincent *et al.*, 2017). However, this finding in the ALT group was less expected. These data illustrate the need to examine the spectral features that are contributing to the separation of these "responders" to determine if there is a consistent pathway or process that is sensitive to the effects of hypobaria and/or hyperoxia.

As a preliminary research effort, this study was successful in generating an altitude chamber system capable of the extreme conditions of hypobaric pressures equivalent to greater than 30,000-feet and delivering 100 percent O_2 safely and effectively to a rodent model. It was determined that rats are tolerant of hypobaric and hyperoxic exposure, particularly within the limited time frame selected for this effort. In spite of the minimal effects and low magnitude of changes seen in brain, heart and lung tissue, it was apparent that a cellular response was in effect as a result of these exposures. Both hypobaric and hyperoxic exposures triggered changes in markers of stress and inflammation, as well as various proteins and lipids. Because of the mild nature of the exposure, it can be estimated that these responses are, for the most part, adaptive and homeostasis can be restored at some point. Within the CNS (central nervous system) damaged nerve tissue normally elicits a graded response that relates to the severity of the injury (Raivich *et al.*, 1999), an elegant system that uses the minimum required response. However, the transition from adaptive to adverse response in tissues like the brain is a blurred line, and the ability to re-establish homeostasis can be impaired. Because of this, follow on studies have been proposed to increase the intensity of the hypobaric and hyperoxic exposures by increasing the duration and number of repeats. It is expected that the change in intensity will augment the effects observed, allowing for more definitive connections with the signaling pathways and biological processes that are impacted. Ultimately, the objective is to provide more information regarding the mechanistic basis of the adverse effects of high altitude flight-like conditions. Understanding the changes at the cellular and molecular level after exposure to these extreme stressors can provide pivotal knowledge about the early events leading to permanent neurological changes. The potential payoff of the knowledge gained from these studies is a better approach to mitigating or preventing operational risks and long-term adverse health outcomes associated with high-altitude flight.

6.0 REFERENCES

Anderson, P.E., Mahle, D.A., Doom, T.E., Reo, N.V., DelRaso, N.J. and Raymer, M.L. 2010. Dynamic adaptive binning: an improved quantification technique for NMR spectroscopic data. Metabolomics. DOI 10.1007/s11306-010-0242-7.

AVMA. 2013. AVMA Guidelines for the Euthanasia of Animals: 2013 Edition. Schaumburg IL: American Veterinary Medical Association. https://www.avma.org/KB/Policies/Documents/euthanasia.pdf.

Bjorkhem, I. and Meaney, S. 2004. Brain cholesterol: Long secret life behind a barrier. Arterioscler Thromb Vasc Bio. 24(5): 806-815.

Forgacs, A.L., Kent, M.N., Makley, M.K., Mets, B., DelRaso, N., Jahns, G.L., Burgoon, L.D., Zacharewski, T.R. and Reo, N.V. 2012. Comparative metabolomic and genomic analyses of TCDD-elicited metabolic disruption in mouse and rat liver. Toxicol Sci. 125(1): 41-55.

Gilmore, T.D. 2006. Introduction to NF-κB: players, pathways, perspectives. Oncogene. 25(51): 6680-6684.

Halliday, K.R, Fenoglio-Preiser, C. and Sillerud, L.O. 1988. Differentiation of human tumors from nonmalignant tissue by natural-abundance 13C NMR spectroscopy. Magn Reson Med. 7: 384-411.

Halliwell, B. 2006. Oxidative stress and neurodegeneration: Where are we now? J Neurochem. 97: 1634-58.

Hensley, K., Fedynshyn, J., Ferrell, S., Floyd, R.A., Gordon, B., Grammas, P., Hamdheydari, L., Mhatre, M., Mou, S., Pye, Q.N., Stewart, C., West, M., West, S. and Williamson, K.S. 2003. Message and protein-level elevation of tumor necrosis factor α (TNFα) and TNFα-modulating cytokines in spinal cords of the G93A-SOD1 mouse model for amyotrophic lateral sclerosis. Neurobiology of Disease. 14:74-80.

Huang, D.W., Sherman, B.T., Lempicki, R.A. 2009a. Systematic and integrative analysis of large gene lists using DAVID Bioinformatics Resources. Nature Protoc. 4(1):44-57.

Huang, D.W., Sherman, B.T., Lempicki, R.A. 2009b. Bioinformatics enrichment tools: paths toward the comprehensive functional analysis of large gene lists. Nucleic Acids Res. 37(1):1-13.

Huang, Y., Zhang, W., Lin, L, Feng, J, Chen, F., Wei, W., Zhao, X., Guo, W., Li, J., Yin, W. and Li, L. 2010. Is endothelial dysfunction of cerebral small vessel responsible for white matter lesions after chronic hypoperfusion in rats? J Neurol Sciences. 299:72-80.

McGuire, S., Sherman, P., Profenna, L., Grogan, P., Sladky, J., Brown, A., Robinson, A., Rowland, L., Hong, E., Patel, B., Tate, D., Kawano, E.S., Fox, P. and Kochunov, P. 2013. White matter hyperintensities on MRI in high altitude U-2 pilots. Neurology. 81(8):729-35.

McGuire, S.A., Sherman, P.M., Brown, A.C., Robinson, A.Y., Tate, D.F., Fox, P.T. and Kochunov, P.V. 2012. Hyperintense white matter lesions in 50 high-altitude pilots with neurologic decompression sickness. Aviat Space Environ Med. 83(12):1117-1122.

McGuire, S.A., Tate, D.F., Wood, J., Sladky, J.H., McDonald, K., Sherman, P.M., Kawano, E.S., Rowland, L.M., Patel, B., Wright, S.N., Hong, E., Rasmussen, J., Willis, A.M. and Kochunov P.V. 2014. Lower neurocognitive function in U-2 pilots: Relationship to white matter hyperintensities. Neurology. 83(7): 638-45

Meneses, P. and Glonek, T. 1988. High resolution 31P NMR of extracted phospholipids. J Lipid Res. 29(5): 679-89.

NRC. 2011. Guide for the Care and Use of Laboratory Animals. Eighth Edition. National Academy Press, Washington, D.C.: Institute of Laboratory Animal Resources, Commission on Life Sciences, National Research Council.

Raivich, G., Bohatschek, M., Kloss, C.U.A., Werner, A., Jones, L.L and Kreutzberg, G.W. 1999. Neuroglial activation repertoire in the injured brain: graded response, molecular mechanisms and cues to physiological function. Brain Res Rev. 30:77-105.

Sillerud, L.O., Han, C.H., Bitensky, M.W. and Francendese, A.A. 1986. Metabolism and structure of triacylglycerols in rat epididymal fat pad adipocytes determined by 13C nuclear magnetic resonance. J Biol Chem. 261: 4380-8.

Stys, P.K., Ransom, B.R, Waxman, S.G. and Davis, P.K. 1990. Role of extracellular calcium in anoxic injury of mammalian central white matter. Proc Natl Acad Sci U S A. 87(11): 4212-6.

Tyagi, R.K., Azrad, A., Degani, H. and Salomon, Y. 1996. Simultaneous extraction of cellular lipids and water-soluble metabolites: evaluation by NMR spectroscopy. Magnet Reson Med. 35: 194-200.

Tyanova, S, Temu, T., Sinitcyn, P., Carlson, A., Hein, M.Y., Geiger, T., Mann, M. and Cox, J. 2016b. The Perseus computational platform for comprehensive analysis of (prote)omics data. Nature Methods. 13: 731–740.

Tyanova, S., Temu, T. and Cox, J. 2016a. The MaxQuant computational platform for mass spectrometry-based shotgun proteomics. Nature Protocols. 11: 2301–2319.

Vincent, J.L., Taccone, F.S. and He, X. 2017. Harmful Effects of Hyperoxia in Postcardiac Arrest, Sepsis, Traumatic Brain Injury, or Stroke: The Importance of Individualized Oxygen Therapy in Critically Ill Patients. Canadian respiratory journal. 2017: 2834956.

Yatomi, Y., Tanaka, R., Shimura, H., Miyamoto, N., Yamashiro, K., Takanashi, M., Urabe, T. and Hattori, N. 2013. Chronic brain ischemia induces the expression of glial glutamate transporter EAAT2 in subcortical white matter. Neuroscience. 244: 113-21

Zhi-Hua, C. and Etsuo, N. 2006. 4-Hydroxynonenol (4-HNE) has been widely accepted as an inducer of oxidative stress. Is this the whole truth about it or can 4-HNE also exert protective effects? IUBMB Life. 58(5-6) 372-373.

LIST OF ACRONYMS

^{13}C	carbon 13
^{1}H	proton
^{31}P	phosphorous 31
8-isoP	8-isoprostane
9-ONA	9-oxononanoic acid
AGC	automatic gain control
ALT	altitude
BS	brainstem
CB	cerebellum
$CDCl_3$	deuterated chloroform
cDNA	complementary deoxyribonucleic acid
$CHCl_3$	chloroform
CID	collision-induced dissociation
CRP	c reactive protein
Cs_2(EDTA)	cesium ethylene diamine tetraacetic acid
CTL	control
CNS	central nervous system
CX	cortex
D_2O	deuterated water
DCS	decompression sickness
ddH_2O	double distilled water
DNA	deoxyribonucleic acid
dNTP	deoxynucleotide triphosphate
ELISA	enzyme linked immunosorbent assay
FA	fatty acid
HP	hippocampus
HNE	4-hydroxynonenol
HPLC	high performance liquid chromatography
HYP	hyperoxia
Hz	hertz
IFN-γ	interferon gamma
IL-6	interleukin 6
kHz	kilohertz
LC	liquid chromatography
LC-MS/MS	liquid chromatography tandem mass spectrometry
MDA	malondialdehyde
MeOH	methanol
MHz	megahertz
MRI	magnetic resonance imaging
mRNA	messenger ribonucleic acid
NDCS	neurological decompression sickness
NFκ-B	nuclear factor kappa B
NMR	nuclear magnetic resonance
NOE	nuclear Overhauser enhancement

OPLS-DA	orthogonal projections onto latent surfaces discriminant analysis
PC1	first principal component
PC2	second principal component
PCA	principal component analysis
PCR	polymerase chain reaction
PUFA	polyunsaturated fatty acid
RIA	radioimmunoassay
RNA	ribonucleic acid
rpm	revolutions per minute
RT	reverse transcription
SCX	strong cation exchange
SD	Sprague Dawley
SEM	standard error of the mean
TMT	tandem mass tags
TNF-α	tumor necrosis factor alpha
TPP	triphenyl phosphate
TSP	2, 2`, 3, 3`-deuterotrimethylsilylpropionic acid
USAFSAM	United States Air Force School of Aerospace Medicine
WMH	white matter hyperintensity